สมบัติเชิงโครงสร้างและเชิงพลวัตของโดเมนรับรู้ความต่างศักย์ของโพแทสเซียมแชนนัลในสถานะ
กระตุ้นและสถานะพักในลิพิดไบเลเยอร์โดยการจำลองพลวัตเชิงโมเลกุล

นางสาวสุนิตย์ ฟูกลาง

STRUCTURAL AND DYNAMICAL PROPERTIES OF VOLTAGE SENSOR DOMAIN OF ACTIVATED AND RESTING POTASSIUM CHANNEL IN LIPID BILAYER BY MOLECULAR DYNAMICS SIMULATION

Miss Sunit Fuklang

A Thesis Submitted in Partial Fulfillment of the Requirements
for the Degree of Master of Science Program in Chemistry
Department of Chemistry
Faculty of Science
Chulalongkorn University
Academic Year 2012
Copyright of Chulalongkorn University

Thesis Title	STRUCRARAL AND DYNAMICAL PROPERTIES OF VOLTAGE SENSOR DOMAIN OF ACTIVATED AND RESTING POTASSIUM CHANNAL IN LIPID BILAYER BY MOLECULAR DYNAMICS SIMULATION
By	Miss Sunit Fuklang
Field of Study	Chemistry
Thesis Advisor	Associate Professor Pornthep Sompornpisut, Ph.D.

Accepted by the Faculty of Science, Chulalongkorn University in Partial Fulfillment of the Requirements for the Master's Degree

....Dean of the Faculty of Science
(Professor Supot Hannongbua, Dr.rer.nat.)

THESIS COMMITTEE

....Chairman
(Assistant Professor Warinthorn Chavasiri, Ph.D.)

....Thesis Advisor
(Associate Professor Pornthep Sompornpisut, Ph.D.)

....Examiner
(Associate Professor Sirirat Kokpol, Ph.D.)

....External Examiner
(Onjira Aruksakunwong, Ph.D.)

สุนิตย์ ฟูกลาง : สมบัติเชิงโครงสร้างและเชิงพลวัตของโดเมนรับรู้ความต่างศักย์ของ
โพแทสเซียมแชนนัลในสถานะกระตุ้นและสถานะพักในลิพิดไบเลเยอร์โดยการจำลอง
พลวัตเชิงโมเลกุล (STRUCTURAL AND DYNAMICAL PROPERTIES OF VOLTAGE
SENSOR DOMAIN OF ACTIVATED AND RESTING POTASSIUM CHANNEL IN
LIPID BILAYER BY MOLECULAR DYNAMICS SIMULATION) อ.ที่ปรึกษา
วิทยานิพนธ์หลัก: รศ.ดร. พรเทพ สมพรพิสุทธิ์, 81 หน้า

โวลเทจเกทไอออนแชนนัลรับรู้การเปลี่ยนแปลงในสนามประจุของทรานสเมมเบรนโดยการจัด
วางตำแหน่งของกลุ่มกรดอะมิโนชนิดประจุบวกโดยเฉพาะอาร์จินีน ซึ่งอยู่ตามท่อนเกลียว S4 ของโดเมน
รับรู้ความต่างศักย์ (VSD) นัยสำคัญหลักของการเคลื่อนที่ของ S4 คือทำให้เกทที่อยู่ในโดเมนโพรงของ
แชนนัลเปิดหรือปิดเพื่อตอบสนองการเปลี่ยนแปลงศักย์ไฟฟ้าของเมมเบรน ความเข้าใจเกี่ยวกับกลไก
ระดับโมเลกุลของการเปลี่ยนคอนฟอร์เมชันที่ขึ้นกับความต่างศักย์นี้ยังขาดความชัดเจน เป็นที่น่าเสียดาย
ที่โครงสร้างผลึกของโวลเทจเกทไอออนแชนนัลที่มีอยู่ ได้แก่ Kv1.2, KvAP, NavAb และ NavRh ใช้แทน
โดเมนรับรู้ความต่างศักย์ได้เพียงสถานะเดียวเท่านั้น นั่นคือคอนฟอร์เมชันในสถานะกระตุ้นหรือ "Up" ใน
วิทยานิพนธ์นี้ นำเสนอการศึกษาเชิงคำนวณของคอนฟอร์เมชันในสถานะกระตุ้น (Up) และสถานะพัก
(Down) ของส่วนโดเมนรับรู้ความต่างศักย์จาก KvAP ซึ่งเป็นโพแทสเซียมแชนนัลของเซลล์โพรคาริโอต
การสร้างแบบจำลองในสถานะพัก อาศัยกระบวนการ PaDSAR การคำนวณพลวัติเชิงโมเลกุล และการ
คำนวณเกททิงชาร์จด้วยวิธีโซลเวนท์คอนทีนิวอัม ผลการศึกษาแสดงการเปลี่ยนคอนฟอร์เมชันของ
KvAP-VSD จากสถานะพักไปสู่สถานะกระตุ้นโดยท่อนเกลียว S4 เอียงและไถลขึ้นไปทางด้านบนของ
เมมเบรนไบเลย์เป็นระยะทางระหว่าง 3 ถึง 5 อังสตรอม การเคลื่อนที่นี้เชื่อมโยงกับการเคลื่อนไหวของ
เกททิงชาร์จอาร์จินีนและการเปลี่ยนของ Salt-bridge ของอาร์จินีน ซึ่งทำให้โมเลกุลน้ำแทรกเข้าไปใน
แกนของโดเมนรับรู้ความต่างศักย์ได้มากขึ้น การปรับทิศของไดโพลบน S4 และการเปลี่ยนของค่าคงที่
ไดอิเล็กตริกภายในโดเมนรับรู้ความต่างศักย์น่าจะเกี่ยวข้องกับกลไกการรับรู้ความต่างศักย์ การ
เปรียบเทียบของการจำลองที่มีและไม่มีสนามประจุภายนอกแสดงให้เห็นว่าการมีอยู่ของศักย์ไฟฟ้าเมม
เบรนช่วยเพิ่มความเสถียรให้กับคอนฟอร์เมชันของ KvAP-VSD ในสถานะพัก การคำนวณเกททิงชาร์จต่อ
มอนอเมอร์ของแบบจำลองให้ค่าเท่ากับ 2.82±0.09e ค่าที่ได้นี้สอดคล้องเป็นอย่างดีกับการทดลองของ
โพแทสเซียมแชนนัลจาก Shaker ในสภาพเตตระเมอร์ ซึ่งวัดได้ค่าประมาณระหว่าง 12-14e

ภาควิชา   เคมี   ลายมือชื่อนิสิต
สาขาวิชา   เคมี   ลายมือชื่อ อ.ที่ปรึกษาวิทยานิพนธ์หลัก
ปีการศึกษา   2555

\# \# 53760323 : MAJOR CHEMISTRY
KEYWORDS : PAPER-BASED DEVICES / SPRAYING METHOD / ACRYLIC LACQUER / NICKEL / DIFFERENTIAL PULSE ANODIC STRIPPING VOLTAMMETRY (DPASV)

SUNIT FUKLANG: STRUCTURAL AND DYNAMICAL PROPERTIES OF VOLTAGE SENSOR DOMAIN OF ACTIVATED AND RESTING POTASSIUM CHANNEL IN LIPID BILAYER BY MOLECULAR DYNAMICS SIMULATION. ADVISOR : ASSOC. PROF., PORNTHEP SOMPORNPISUT, Ph.D., 81 pp.

Voltage-gated ion channels sense changes in transmembrane electric fields by the rearrangement of the positively charged residues, predominantly arginines, along the S4 helix in the voltage-sensing domain (VSD). The key significance for the S4 motion is to drive the gate located in the pore domain of the channels opening or closing in respond to changes in the membrane potential. The molecular mechanism of voltage-dependent conformational transition of VSD is not clearly understood. Unfortunately, crystal structures of a number of voltage-gated ion channels including Kv1.2, KvAP, NavAb and NavRh, could represent the voltage sensor in an only one state so-called "Up" or activated conformation. In this thesis, a computational study of the activated (Up) and resting (Down) conformations of the isolated VSD from the prokaryotic K^+ channel KvAP is presented. The Down sensor model was developed based on the PaDSAR approach, molecular dynamics simulations and solvent continuum gating charge calculations. The results show that KvAP-VSD transforms from the resting to activated conformations by an upward tilt and slide of the S4 helix to the upper face of membrane bilayer with a distance of 3-5Å. This motion was associated with the movement of gating charge arginines and a change in salt-bridge arginines, giving rise to an increase of water penetration into the voltage sensor core. The reorientation of helical dipoles on S4 and a change in the internal dielectric constant of VSD should involve with the voltage-sensing mechanism. Comparison of the simulations with and without external electric fields revealed that the presence of membrane potential helps to stabilize the Down conformation of KvAP-VSD. The gating charge for the models was calculated to be 2.82±0.09e per monomer. This is in good agreement with the experimental estimates of 12–14e measured for the Shaker K^+ tetrameric channel.

Department : __Chemistry_____ Student's Signature_____

Field of Study : __Chemistry_____ Advisor's Signature_____

Academic Year : _2012_____

ACKNOWLEDGEMENTS

CONTENTS

LIST OF TABLES

LIST OF FIGURES

FIGURE   **PAGE**

LIST OF ABBREVIATIONS

K_v	voltage-gated potassium channels
Na_v	voltage-gated sodium channels
Ca_v	voltage-gated calcium channels
VSD	voltage sensor domain
PD	pore domain
TM	transmembrane
NaChBac	sodium channels of the bacterium *Bacillus Halodurans*
KvAP	voltage-dependent potassium channel from *Aeropyrum pernix*
Ci – VSP	*Ciona intestinalis* voltage-sensitive phosphatase
Å	angstrom
º	degree
MD	molecular dynamics
PDB	protein data bank
PSF	protein structure file
VMD	visual molecular dynamics
APBS	adaptive Poisson-Boltzmann solver
PBE	Poisson-Boltzmann equation
PaDSAR	pseudoatom-driven solvent accessibility refinement
EPR	electron paramagnetic resonance
α	alpha
SDSL	site directed spin labeling
R	arginine acid
D	aspartic acid
E	glutamic acid

ΔG_{elec}	electrostatic salvation free energy
L_{mem}	range of membrane bilayer thickness
ε_m	dielectric constant of the membrane
ε_w	dielectric constant of the water
$\varepsilon_{protein}$	dielectric constant of the protein
POPC	palmitoyl oleoyl phosphatidyl cholines
DOTAP	dioleoyltrimethylammonium-propane
ns	nanosecond
RMSD	root-mean-square-deviation
RMSF	root-mean-square-fluctuation
3D	three dimensional
Kcal	kilocalorie
mV	milivolt
DSSP	database of secondary structure assignments of all protein

CHAPTER I

INTRODUCTION

1.1 Cell membranes

The cell membrane or plasma membrane is a selectively permeable membrane that encircles the cytoplasm of living organisms to protect the intracellular organelle from its extracellular surroundings. The cell membrane function is cell to cell communication by controlling the specific molecules what goes in and out of across the cells [1]. Therefore cell membranes are associated with a variety of mechanical supports for cellular processes such as cell adhesion, ion conductivity and cell signaling [2]. The major constituents of the cell membrane are proteins and lipids [3]. Especially the common lipid in most membranes are phospholipid. They are arranged as a bilayer in "the fluid mosaic model". The membrane is a mosaic of protein molecules bobbing in a fluid bilayer of phospholipid. One of the most widely studied proteins that are embedded in the lipid bilayer is called membrane protein channels [4].
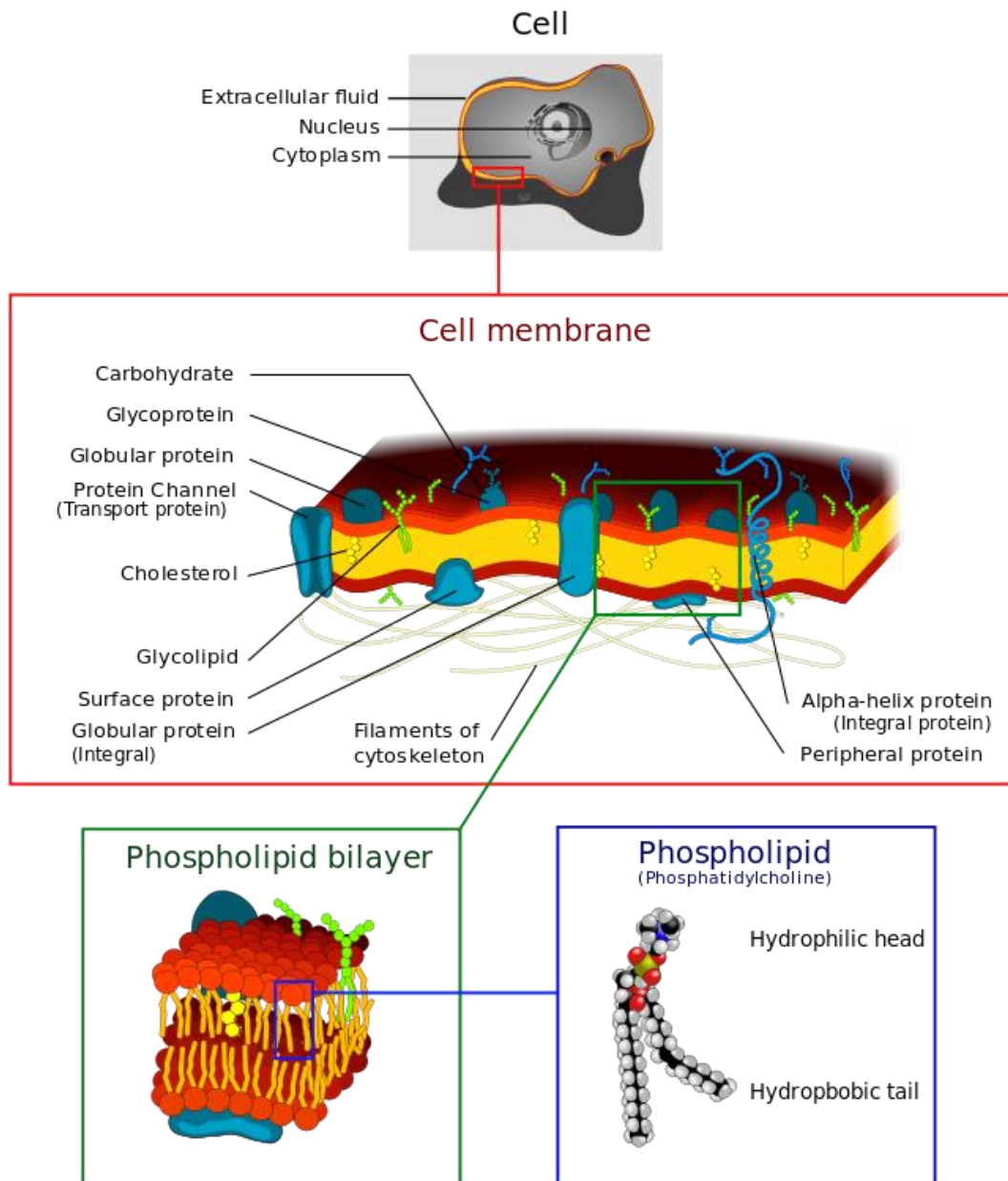
Figure 1.1 The fluid mosaic model representation of cell membrane or plasma membrane structure, the membrane proteins are embedded in double layer, is an amphipathic molecules, arranged with the hydrophilic heads are exposed to the outside of high content water region while the lipophilic tails facing each other [4].

1.2 Ion transport across cell membranes

Ions that are too polar to diffuse across the membrane lipid must be transported by a special group of membrane proteins such as carriers, channels and transporters [5]. A general classification of ion transport mechanisms across cell membrane can be loosely categorized into passive transport and active transport [2].

Passive transport is the movement of ions across cell membranes down an electrochemical gradient. This spontaneous process is the net passive movement of particles from one side of the membrane with a higher concentration of solute to the other side with a low concentration. The direction of the chemical gradient is downhill. Examples of passive transport include passive diffusion, ion channels, and facilitated diffusion. Channel proteins typically form a narrow pore and carry out passive transport, in which the movement of specific solute based on concentration gradient from high to low concentration [6-7].

Active transport is the movement of ions across cell membranes against a concentration gradient. This process of ion transport is not spontaneous in forward direction but the reverse process is spontaneous. This means that active transport requires energy to drive the process because ions are transported from a region of lower concentration to one of higher concentration. Energy input can be derived from a variety of sources such as hydrolysis of ATP and light. Membrane proteins that transport ion through the active transport process are referred as pump, for instance, Na/K pump, ATP-dependent pumps and light-driven pumps [8-10].

1.3 Ion Channels

Ion channels are a large integral membrane protein complex found in all living cells. They allow the movement of ions across cell membranes [11-12]. Their functions include signal transduction and regulation of many physiological processes, maintaining the resting membrane potential and modulating electrical excitability in neuron and muscle cells [13-14]. Generally, ion channels are often found as multimeric proteins [15]. Each monomer may be composed of one or more membrane-spanning polypeptide segments called transmembrane domain [16-17],

which play a crucial role for ion channel function as well as stability of local and global fold structures. An arrangement of multi-subunit transmembrane complex results in ion-conductive pore which provides a hydrophilic pathway for ions to across the hydrophobic membrane [18-19].

Ion channels are characterized by the ability to open and close in response to electrical, chemical or mechanical stimuli [19]. There are many types of ion channels. Generally, they can be classified on the basis of external stimuli (Figure 1.2). For instance voltage-gated ion channels opens and closes the pore in respond to changes in membrane potential between the inside and outside of cells. Ligand-gated ion channels are the class that has ligand-binding domain. Ligand binding site may be located in either extracellular or intracellular sides of cell membranes. The binding of small ligand molecules can trigger the channel to change the conformation from the close to open states. Examples of this class of ion channels include neurotransmitter acetylcholine receptor or ATP-gated channels. Mechanosensitive ion channel is a class of ion channels that can be activated by mechanical stimuli [20]. This class of ion channels contains a sensory domain that responses to touch, vibration, compression or stretch. For example, a mechanosensitive ion channel of large conductance is activated by changes in osmotic stretch [21].
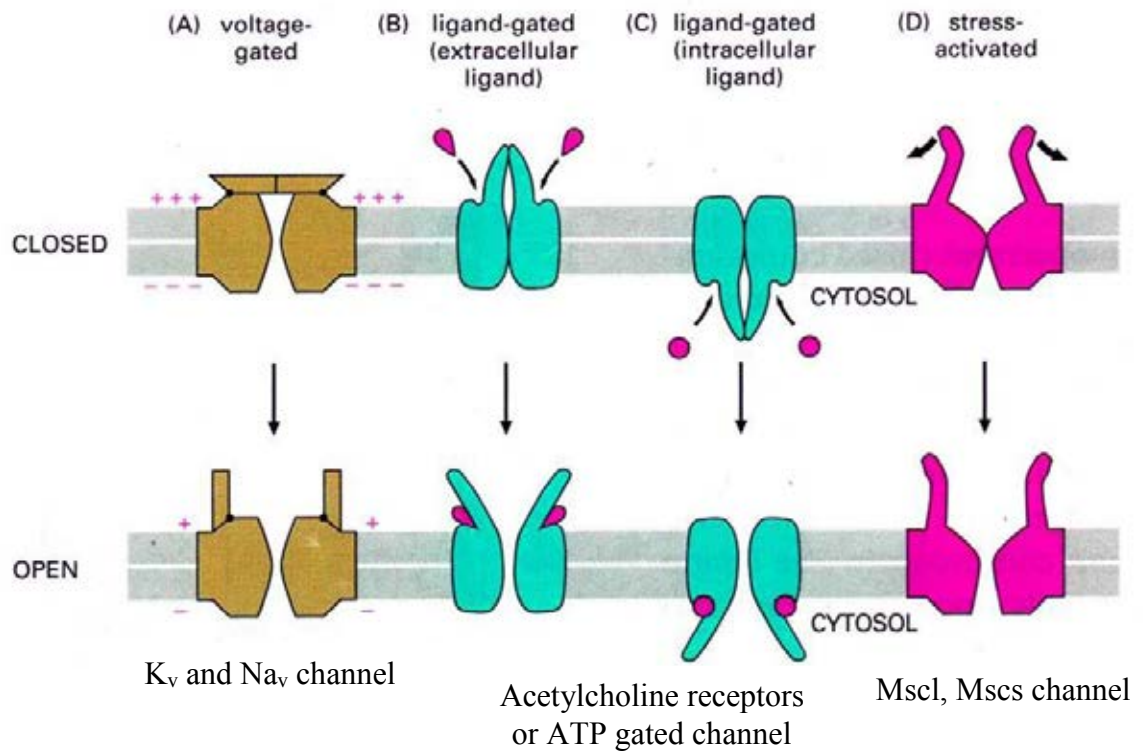
Figure 1.2 Various type of ion channels A) voltage-gated ion channels B- C) ligand-gated ion channels and D) mechanically gated ion channels [20].

1.4 Voltage-gated ion channels

Three major types of voltage-gated or voltage-dependent ion channels are voltage-gated sodium channels (Na_v), voltage-gated calcium channels (Ca_v) and voltage-gated potassium channels (K_v) [29]. K_v and Na_v are responsible for generation and propagation of action potential in neurons and other excitable cells [30]. Ca_v serve an important role in signal transduction by initiating release of neurotransmitters at synapses [15-16, 21]. K_v, Na_v and Ca_v are cation-selective channels [31]. They share a common structural architecture, with which the channels are made of two separate domains, the voltage sensor and central pore domains [16, 32]. The voltage-sensing unit is responsible for the detection of electrical potential changes due to electrochemical gradient between intracellular and extracellular solution. The movement of the voltage sensor in response to membrane voltage changes drives the

pore conformation to open (activated) or close (resting) the gate located within the pore [33-34].
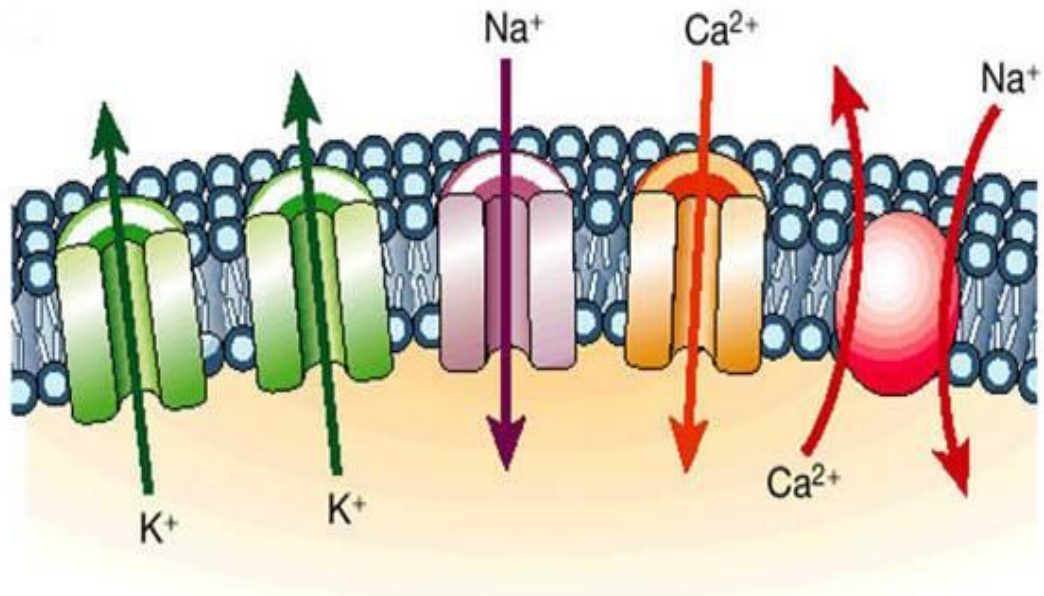
Figure 1.3 Voltage-gated ion channels function as pores to permit the flux of ions down their electrochemical potential gradient [30].

1.5 The action potential

The action potential in neurons is the electrical impulse generated from electrochemical gradients of ions, particularly, sodium and potassium ions [22], between extracellular and intracellular side of membrane. Changes in electrical potential are due to the movement of ions through membrane conductances called voltage-dependent ion channels [23-24]. The conductance of these ion channels (G), is related with the current flowing across the membrane (I) and the electrical potential across the membrane (V_m) as.

$$I_x = G \times (V_m - V_x) \tag{1.1}$$

Where V_x is the equilibrium potential for the x ion, given by the Nernst equation:

$$V_x = \left(\frac{RT}{z_x F}\right)\ln\left(\frac{c_{out}}{c_{in}}\right) \tag{1.2}$$

Where R = 8.314 J (mol K) is the gas constant, T is absolute temperature, z_x is the valence of ion x, F = 9.648×104 C/mol is Faraday's constant, c_{out} is the outer concentration of ion x, and c_{in} is the inner concentration of ion x [24-26].

The action potential is governed by change in the rising and falling of electrical membrane potential which is predominantly controlled by the opening and closing of K_v and Na_v channels (Figure 1.4) [26]. At the resting state, the membrane potential, which is the voltage difference across the neural membrane, is typically in a range from -40 to -90 mV [23]. Both K_v and Na_v channels are in close state, and therefore K^+ and Na^+ cannot across the membrane. When the nervous cells are stimulated, membrane potential becomes less negative due to the passage of positive electrical current into the cell. This is because Na_v channels open and Na^+ rapidly influx inside cell. The rising phase of action potential is called depolarization stage. The inward flow of Na^+ is followed by the opening of K_v that permit the outward flow of K^+. When the membrane potential reaches the highest peak of the action potential, the falling phase of the action potential comes to play [24]. There are two predominant factors that cause a drop in the action potential. Na_v gates are closed whereas K_v gates still open. The efflux of K^+ and no influx of Na^+ result in a decrease of the membrane potential. This state is called repolarization stage. When the voltage potential is reduced to less than the resting state, this changing state is called hyperpolarization, as shown in Figure 1.4. At this state, all Na_v and K_v channels are inactive and no ion flows through these channels. After hyperpolarization, the Na-K pump returns the voltage potential back to the resting potential again [24, 27].
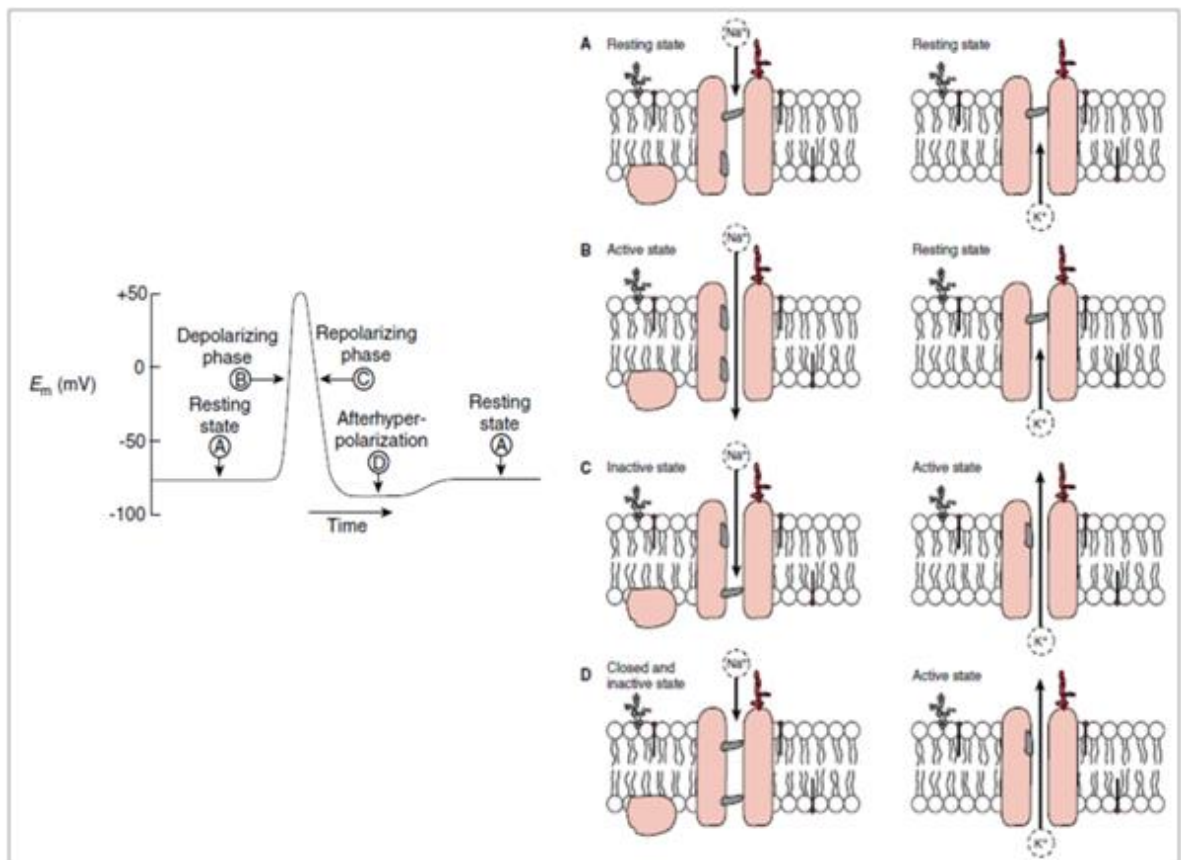
Figure 1.4 The states of voltage-gated sodium and potassium channels correlated during the course of the action potential [28].

1.6 Voltage-gated potassium channels

Voltage-gated potassium channels (K_v) are a key component to generate action potential along the cell membrane of excitable neurons and muscle cells by controlling the flow of K^+ ions through the narrow pore across the membrane bilayer [35-36]. The structure of K_v channels are homotetrameric channels, each subunit or domain composes of six transmembrane α-helices, the first four S1-S4 form the voltage sensor domain (VSD) and the last two S5-S6 form the pore domain (PD), especially S4 contains many positive charge arginine or lysine as a result they sense to change in transmembrane electrical potential [12, 37-38]. Due to the important role of K_v channels correlates with regulating membrane excitability therefore, are also the target on the pharmacological and emerging genetic such as neurotransmitter release system, epithelial electrolyte transport along with smooth muscle contraction [39].

1.7 Crystal structure of a voltage gated potassium channel KvAP

In 2003, Jiang and coworker reported the 3D crystal structure of K_v channel from *Aecheabacteria aeropyrumpernix* (KvAP) [40]. The KvAP channel is a homotetramer. Each subunit consists of six transmembrane α-helices (S1-S6) [33, 41].The KvAP structure reveals the four-fold symmetric arrangement of each subunit. The central pore of the channel is formed by the four-fold symmetric arrangement of the S5-S6 helices. The voltage sensor domain spans from the S1 to S4 helices and is located at the outer perimeter of the pore. The S3 helix is broken into two short helices; S3a and S3b. The S3b and the N-terminal half of S4 helix form helix-turn-helix structure called voltage sensor paddle [40]. The significance of the paddle has been proposed to undergo conformational changes during the channel opening and closing. The S4 segment containing conserved gating charge arginines in every third position are identified as the major voltage sensor element [42-43].
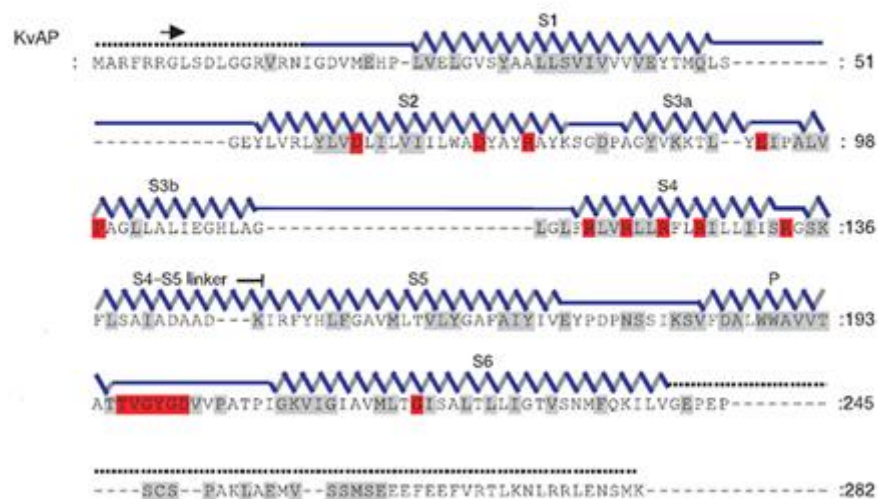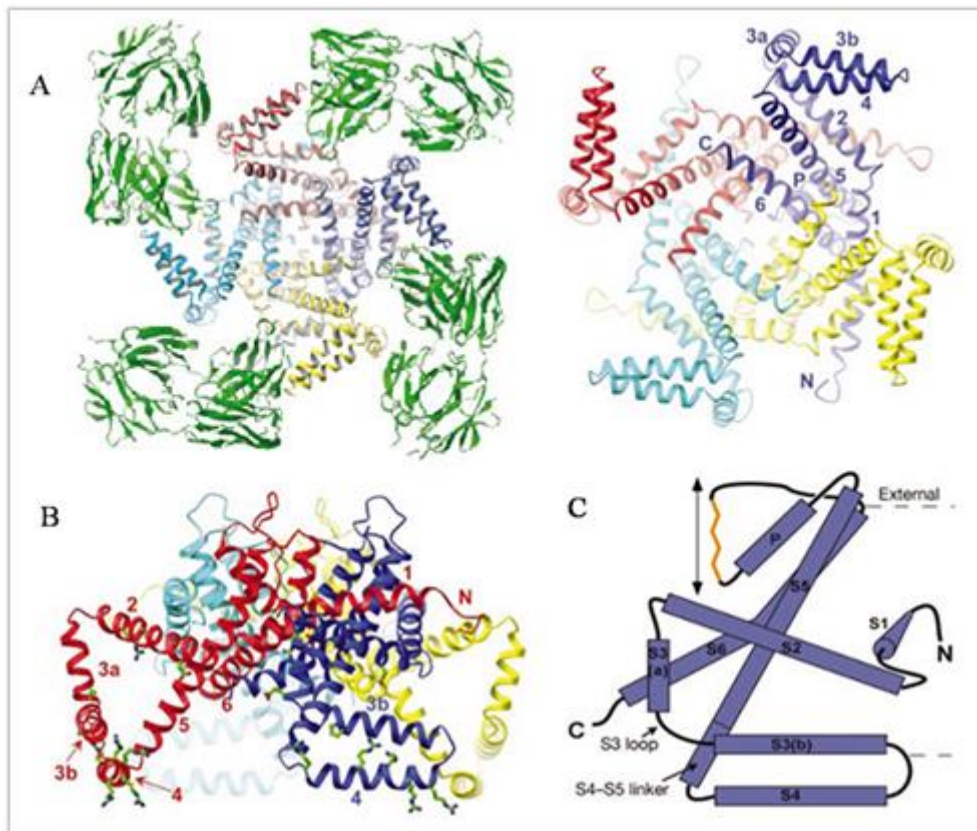
Figure 1.5 The crystal structure of full-length KvAP channel A) the channel tetramer bound to monoclonal fab fragment in green ribbon color viewed from the intracellular solution B) 90º rotation correlate with A, and C) A schematic diagram is shown selectivity filter and an arrow to indicate the ion pathway. E) The amino acid sequence of KvAP [40].
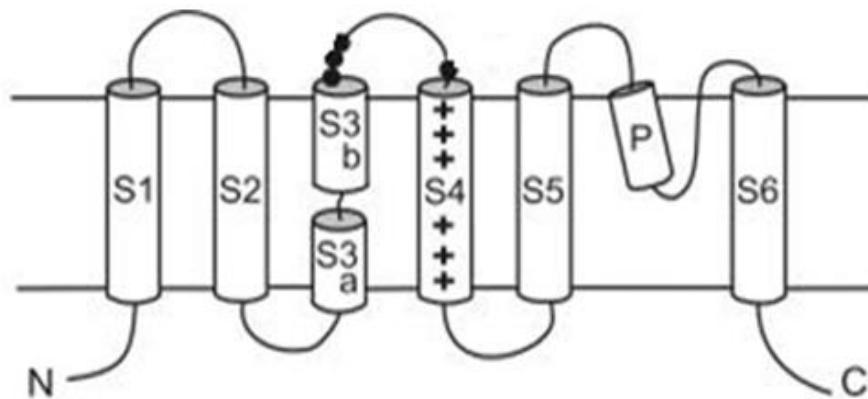
Figure 1.6 Transmembrane topology of KvAP **[44].**

1.8 Voltage sensor domain: the functional independent domain

Voltage-gated ion channel consists of two functional domains, voltage sensor domain and pore domain [16, 32]. It has been found that the isolated voltage sensor domain can perform function without the pore domain, implying a functional independence voltage sensor [38]. This finding has been supported by a number of functional and structural studies. The x-ray structure of the isolated voltage sensor domain of KvAP channel solved at a resolution of 1.9 Å revealed the secondary structures of S1-S4 helices are maintained [40]. In addition, the discovery of novel voltage sensing phosphatase from *C.intestinalis*, a non-channel protein, supports the idea of the functional independent domain of the voltage sensor [45]. Recently, voltage-gated proton channel was identified to contain a voltage sensor domain but its amino acid sequence is not found to be uncorrelated with that of voltage-gated ion channel [46].

1.9 Voltage sensing mechanism: how does the voltage sensor move?

Voltage-dependent ion channels open the gate in response to membrane depolarization by the movement of S4 helix of the VSD [34]. It is believed that the movement of S4 effect to the conformational change of the channel. Although, it is difficult to solve about the gating charge movement in 3D space. However three conceptual models have been proposed (Figure 1.7). Paddle model was proposed on

the basic of crystal structure of KvAP potassium channel by Jiang and cowoker. The S3b and S4 helices packing similar as paddle structure [40, 42]. That tightly contact during the course of complete gating cycle. During the depolarization process, the paddle structure translocated from innerbilayer expose to extracellular surface medium, suggesting S4 charge large translates ~15-20 Å. The general idea of transporter model is changing of positive charge arginine face from intracellular to extracellular by S4 helix translation about 2-3 Å. The last helical screw model represents the S4 helix rotation along its axis and vertical translation ~4.5-5 Å vertical with respect to membrane plane to change the charge exposure from intracellular to extracellular [33, 43] A general feature of three models were a charge translation from inside to outside during the gating process and the distinction among the three models is the magnitude of charge relocation. Up to now, the molecular mechanism underling the voltage dependent conformational changes remain a subject of debates. Unfortunately, crystal structures of a number of voltage-gated ion channels including Kv1.2, KvAP, NavAb and NavRh, could represent the voltage sensor in an only one state so-called "Up" or activated conformation. In this thesis, a computational study of the activated (Up) and resting (Down) conformations of the isolated VSD from the prokaryotic K^+ channel KvAP is presented.
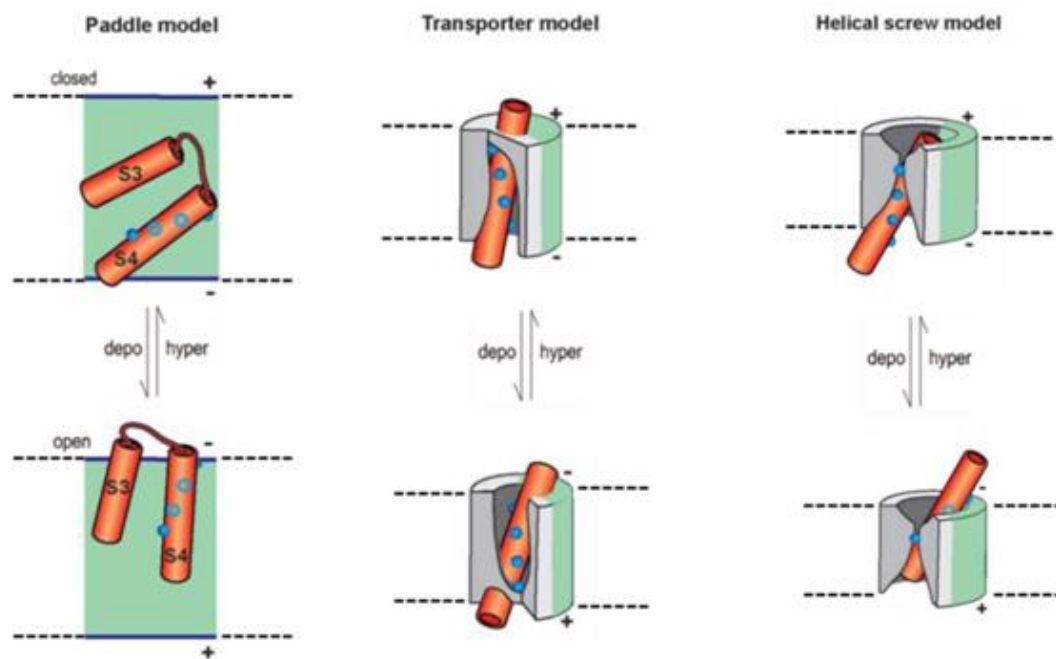
Figure 1.7 The three major concepts of voltage-sensing mechanism [33].

1.10 Objectives

The main purposes of this research are:

1. To construct structural models of the voltage-sensing domain of KvAP channel in activated (Up) and resting (Down) configurations based on a variable experimental data.

2. To investigate structure and dynamic properties of the voltage-sensing domain of KvAP channel in activated (Up) and resting (Down) configurations by using all-atom molecular dynamics simulation.

This thesis is organized as follows. The first chapter is an introduction and some literature reviews on the study of voltage-dependent ion channels. The second chapter describes basic essential of molecular simulations. A list of handout and software is presented in chapter three. The work carried out during the thesis course can be separated into two topics. The chapter four describes a computational of Up and Down state conformations of KvAP voltage sensor. In chapter five the study on evaluation of transmembrane protein position in OPM database using continuum electrostatic approach is reported. Each chapter is a self-constrained chapter, including introduction, method, results, discussion and conclusion.

CHAPTER II

BASIC ESSENTIALS OF MOLECULAR SIMULATIONS

2.1 Molecular dynamics simulations

Molecular simulation technique allows a profound understanding the properties of thermodynamic behavior associated with its structural properties [47-51]. The two important simulation techniques are Monte carlo (MC) and molecular dynamics (MD) [48, 50]. The Monte carlo is a computational-based sampling technique base on a random probability with continuous variables. MC technique creates large numbers of configurations from one specific microscopic configuration or microstate to the next step by sampling the appropriate position, orientation and conformation of the studied system. The advantage of this method is flexibility of choosing an arbitrary function and simulate different ensembles, as well as time saving as the potential energy is required [52].

While molecular dynamics is the most detailed technique by which atomic trajectories of N particles of the system are generated by calculating the motion of individual particle on the basis of solving the numerical integration of Newton's equation [48-49]. Certain positions and velocities of each particle are determined by specific inter-atomic potential energy with a well-defined boundary condition. The second law of the classical Newton's equation is given by [47].

$$m_i \frac{d^2 r_i}{dt^2} = f_i = -\frac{\partial}{\partial r_i} U(r_1, r_2, ..., r_N) \tag{2.1}$$

Where $U(r_1, r_2, ..., r_N)$ is the potential energy as a function of coordinate of N particles. f_i is the force acting on i^{th} atoms. It is determined by the gradient or the first derivative of the potential energy with respect to the position change. Acceleration is expressed in terms of the second derivative of the particle position r with respect to time [53]. This differential equation is computationally solved via the numerical methods. In molecular dynamics, successive configurations is called trajectory that contains time-dependent positions and velocities of the particles in the system

[48-49]. Molecular dynamics trajectory is divided into several small stages with each separated in a fixed time *(Δt)* as shown in Eq. 2.2.

$$r_i(t_0) \rightarrow r_i(t_0 + \Delta t) \rightarrow r_i(t_0 + 2\Delta t) \rightarrow \ldots r_i(t_0 + n\Delta t)$$
(2.2)

A number of integration algorithms using finite difference techniques are employed to solve the Newton's equation. There are many integration algorithms for solving the equation of motion. The choice of the integrators for MD simulation depends on the developer or programmer [54]. For instance, the Verlet algorithm shown in Eq.2.3 illustrated a relation of the positions r_i at the time $t_0 + \Delta t$:

$$r_i(t_0 + \Delta t) = -r_i(t_0 - \Delta t) + 2r_i(t_0) + a_i(t_0)\Delta t^2 + O(\Delta t^4)$$
(2.3)

And the relation of the velocities is expressed as:

$$r_i(t_0) = \frac{1}{2\Delta t}\left[r_i(t_0 + \Delta t) - r_i(t_0 - \Delta t)\right]$$
(2.4)

A widely used algorithm for generating molecular dynamic trajectory is called the leap-frog algorithm [55]:

$$r_i(t_0 + \Delta t) = r_i(t_0) + v_i\left(t_0 + \frac{\Delta t}{2}\right)\Delta t$$
(2.5)

$$v_i\left(t_0 + \frac{\Delta t}{2}\right) = v_i\left(t_0 - \frac{\Delta t}{2}\right) + a_i(t_0)\Delta t$$
(2.6)

The velocity-Verlet algorithm is also an efficient, stable and reasonably accurate algorithm [47]:

$$r_i(t_0 + \Delta t) = r_i(t_0) + v_i(t_0)\Delta t + \frac{1}{2}a_i(t_0)\Delta t^2$$
(2.7)

$$v_i(t_0 + \Delta t) = v_i(t_0) + \frac{1}{2}\left[a_i(t_0 + \Delta t)\right]\Delta t$$
(2.8)

2.2 Force fields

In molecular dynamics simulation of biological systems which often contain several thousands of atoms [48]. A simple "mechanical" molecular model is typically used to describe molecular structures and properties because of the great computational speed. Molecular mechanics methods are generally considered a set of atoms as spheres connected with bonds as springs. Atoms that are greater than two bonds apart can interact through van der Waals attraction, steric repulsion, and electrostatic attraction/repulsion. According to the potential energy of N particles $U\ (r_1, r_2, ... r_n)$ shown in Eq. 2.9 [49].

$$f_i = -\nabla r_i U(r_1, r_2, ... r_N) = -\left(\frac{\partial u}{\partial x_i}, \frac{\partial u}{\partial y_i}, \frac{\partial u}{\partial z_i} \right)_i \qquad (2.9)$$

A simple molecular mechanics energy equation is given by the sum of the individual interaction energy as shown in Eq. 2.10 [49]:

$$U_{(r_1, r_2, ..., r_N)} = (U_{bonds} + U_{angles} + U_{dihedrals})_{bonded} + (U_{elec} + U_{vdw})_{non-bonded} \qquad (2.10)$$

Where U_{bonds}, U_{angles} and $U_{dihedrals}$ are the stretching energy, bending energy and torsion energy, respectively. U_{elec} and U_{vdw} are electrostatic and van der Waals energies, respectively. The Eq 2.1 equation required set of parameters to describe the behavior of different kinds of atoms and bonds that are called a force-field [50-51].

Force field is the mathematical expression that influence of the energy as a function on coordinate of the particles of the system or the correlation between physical property of system and the interatomic force [48-51]. Many different types of force-fields are available and varies upon the choice of the molecular dynamics software package [56]. Here, the common mathematical form of the energy terms will be described.

1.2.1 Bonded interaction

$$U(r_1, \cdots r_N) = \sum_{bonds} \frac{1}{2} k^b \left(r - r^0 \right)^2 + \sum_{angles} \frac{1}{2} k^\theta \left(\theta - \theta^0 \right)^2 + \sum_{dihedrals} k^\phi \left[1 + \cos \left(n\phi - \phi^0 \right) \right] \qquad (2.11)$$

Where k^b, k^θ and k^ϕ are the force constants for bond, angle and dihedral respectively, r^0, θ^0 and ϕ^0 are the equilibrium values of bond length, bond angle and dihedral angle. The first two terms in the right-hand side are the stretching and bending energy terms. They are based on Hooke's law. The force constant k^b and k^θ control the stiffness of the bond and angle springs, respectively [48]. These two energy terms estimates the energy associated with vibration about the equilibrium bond length and bond angle. The last energy term corresponds to the torsion energy which is modeled by a simple periodic cosine function [49-50].
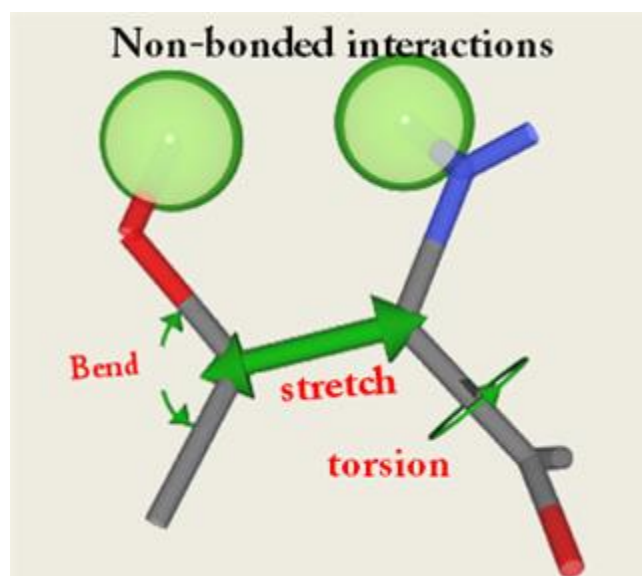
Figure 2.1 Represent the bonded interaction of all atom force field modeling at atomic scale.

1.2.2   Non-bonded interaction

The non-bonded energy represents the sum of pair-wise interaction energies of all possible interacting non-bonded atoms i and j. The non-bonded energy accounts for van der Waals, and electrostatic interactions as shown in Eq. 2.12 [49-51].

$$U(r_i,\ldots r_N)=\Sigma_{LJ}\, 4\varepsilon_{ij}\left(\frac{\sigma_{ij}^{12}}{r_{ij}^{12}}-\frac{\sigma_{ij}^{6}}{\sigma_{ij}^{6}}\right)+\Sigma_{elec}\frac{q_i q_j}{r_{ij}} \tag{2.12}$$

The van der waals interaction term, was proposed a model that combines the attractive and repulsive potential by Lennard – Jones in 1924. Where σ^{12}, σ^{6} are the Lennerd-Jones parameter r_{ij} is a distance between atom i and j [47]. The electrostatic energy term describes the force resulting from the interaction between two partial charge particles q_i and q_j. The energy between atoms i and j is defined by Coulomb's Law [48-49].
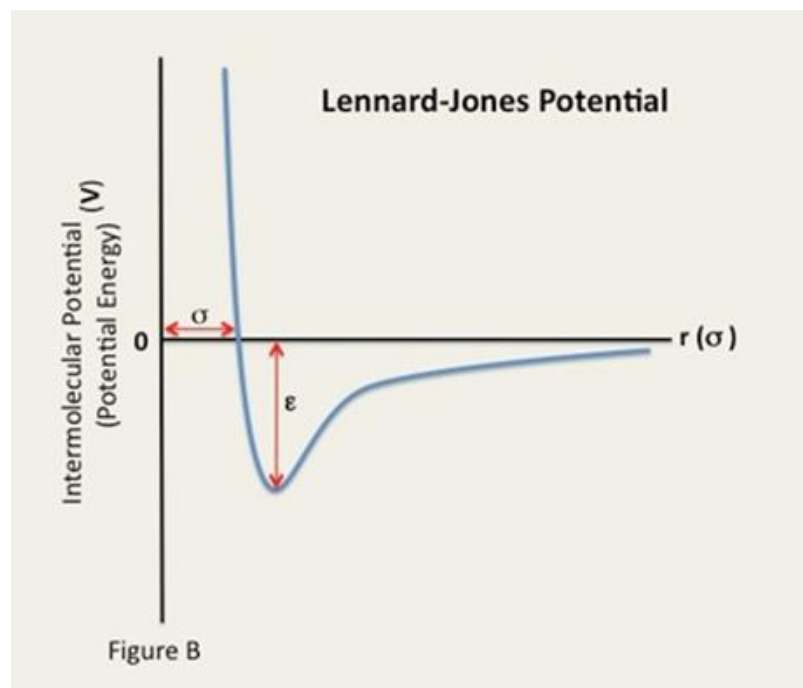
Figure B

Figure 2.2 Lennard-Jones potential.

2.3 Poisson-Boltzmann Solvent Continuum

The electrostatic solvation properties play an important benefit to understand a basic fundamental of many biological processes [57-61]. A variety of computational methods have been developed for describing electrostatic solvation behavior and can be roughly categorized into two different strategies; explicit and implicit solvation models (Figure 2.3) [57-58]. In explicit models, the solvent (water) molecules are placed around the simulated solute (protein) molecule. It is in contrast with implicit models which treat the solvation effects as polarizable continuum media or a mean field charge distribution [58, 62-64].
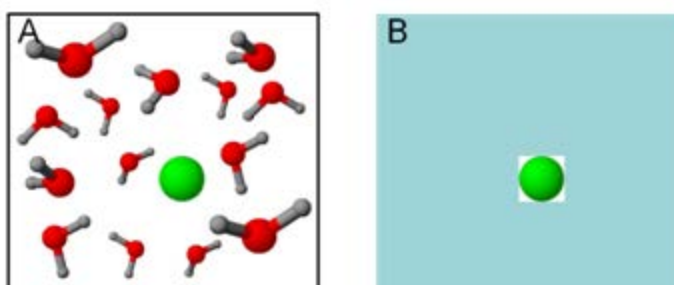
Figure 2.3 Represent two electrostatic solvation models A) the explicit model exposed the solvent in full atomic detail in the system while B) the implicit model exposed the model solvent effect in form of dielectric continuum.

Implicit solvent methods have gained increasing popularity over explicit solvent models because of computational efficiency and simplicity [62]. In implicit solvent models, the biomolecules are examined explicitly and described the solute-solvent interaction in term of solvation free energy [58-59, 62-64], that energy require when transferring the biomolecules from vacuum to high dielectric medium (Figure 2.4) [58, 64]
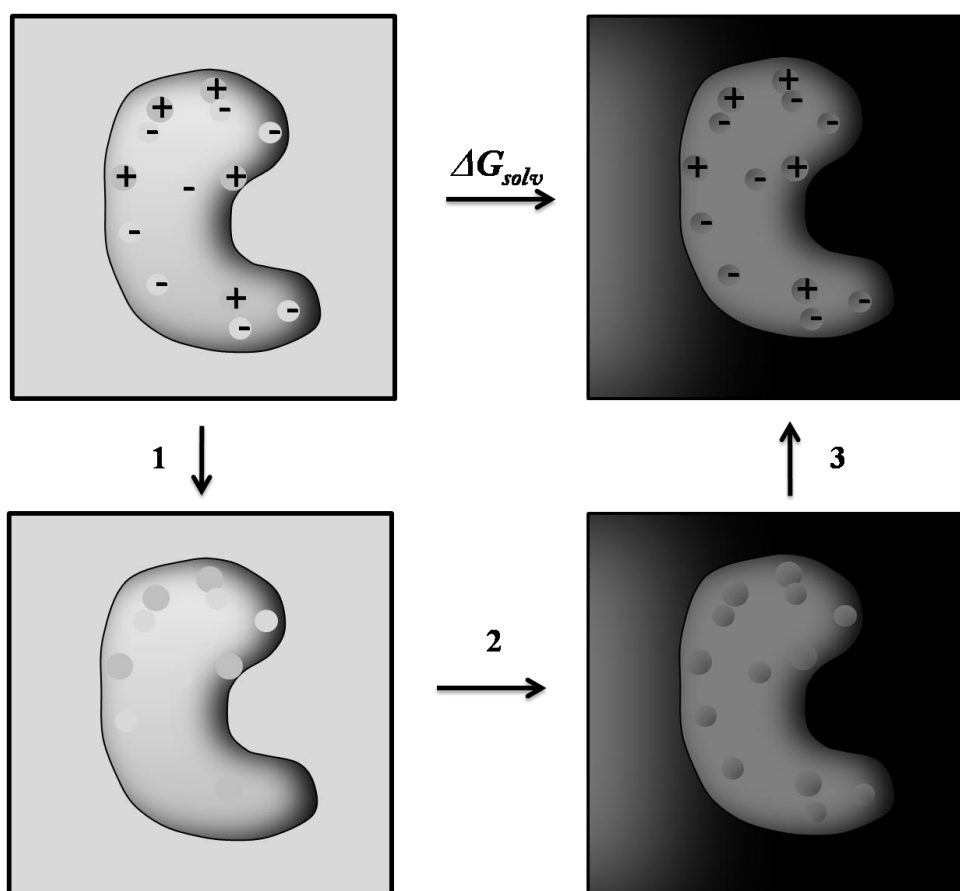
Figure 2.4 A thermodynamic cycle of solvation free energy 1) uncharged solute in vacuum 2) loading the uncharged into high dielectric solvent 3) the solute charges increase back to their normal values. Step 2 is the free energy change of the nonpolar solvation while opposite direction is the polar solvation, present the sum of the energy change of step 1 and 3.

One of the popular implicit solvation method is based on solving the Poisson-Boltzmann (PB) equation [57-63, 65-67]. This equation is derived from a continuous dielectric medium model of biomolecular solution. The Poisson equation explains an electrostatic potential $\emptyset(x)$ in discontinuous dielectric media ε. Owing to a charge distribution, $\rho(x)$ gives rise to an expression [60-61, 67].

$$-\nabla \bullet [\varepsilon(x)\nabla\phi(x)] = 4\pi\rho(x) \tag{2.13}$$

For a system without mobile ions surrounding the solute, the charge distribution is defined as a fixed point charge on center of biomolecule [67].

$$\rho_x(x) = \sum_{i=1}^{M} Q_i \delta(x - x_i)$$ (2.14)

Where Q_i is a charge magnitudes of species i and x_i represents its charge position. Considering a system with mobile ions, their effect is defined by using a mean-field approximation in terms of Boltzmann distribution of m different mobile species [62, 67].

$$\rho_m(x) = e_c \sum_{j=1}^{m} \bar{n}_j z_j \exp\left(-e_c z_j \phi(x)/kT - V_j(x)/kT\right)$$ (2.15)

Where e_c is the elementary charge, V_j is the steric interaction that occurs between biomolecular solute and ion species. $\bar{n}_j$ and z_j are a local concentration and the valence of species j respectively. kT is the thermal energy of the system [62, 67]. Then substitution of two charge densities $\rho_x(x)$ and $\rho_m(x)$ into the Poisson equation gives the nonlinear Poisson-Boltzmann equation [64, 67].

$$-\nabla \bullet [\varepsilon(x)\nabla\phi(x)] = 4\pi\left(\rho_f(x) + \rho_m(x)\right)$$ (2.16)

$$-\nabla \bullet [\varepsilon(x)\nabla\phi(x)] - 4\pi e_c \sum_{j=1}^{} \bar{n}_j z_j \exp\left(-e_c z_j \phi(x)/kT - V_j(x)/kT\right) = 4\pi\sum_{i=1}^{M} Q_i \delta(x - x_i)$$
(2.17)

For a 1:1 electrolyte solution, q_1, $q_2 = 1$, 2 and assume $V_1 = V_2 = V$ then the canonical form of non-linearized equation can be reduced to

$$-\nabla \bullet [\varepsilon(x)\nabla\phi(x)] + 8\pi e_c \bar{n} e^{-v(x)/kT} \sinh[e_c \phi(x)/kT] = 4\pi\sum_{i=1}^{M} Q_i \delta(x - x_i)$$
(2.18)

The linearized Poisson-Boltzmann equation can be written by assuming $e_c\phi(x)kT \ll 1$ from the Toyler expanding for the exponential function can be reduced to Eq.2.19. That present associated between specific term with model charged solute (Figure 2.5) [64, 67]

$$-\nabla \bullet [\varepsilon(x)\nabla\phi(x)] + \overline{k}^2(x)\phi(x) = 4\pi\sum_{i=1}^{M} Q_i \delta(x - x_i) \qquad (2.19)$$

Where $\overline{k}^2(x) = e^{-V(x)/kT} 4\pi \overline{e}_c^2 / kT \sum_s \overline{n}_z z_s^2 = e^{-V(x)/kT} 8\pi \overline{e}_c^2 I / kT$ and $I = \dfrac{1}{2}\sum_s \overline{n}_s z_s^2$ are the ion accessibility parameter and the ionic strength respectively [64, 67]. Eq. 2.19 is the PB equation representing a continuum model of the solvent and counterion environment surrounding a biomolecule. In general, the PB equation is solved in a finite domain with a fixed potential on the defined boundary [67]. The PB equation has become a standard method for elucidating the electrostatic properties in biomolecular simulation.

$$-\nabla\cdot\varepsilon(x)\nabla\phi(x) + \varepsilon\kappa^2(x)\phi(x) = \sum_{i=1}^{N} Q_i \delta(x - x_i)$$
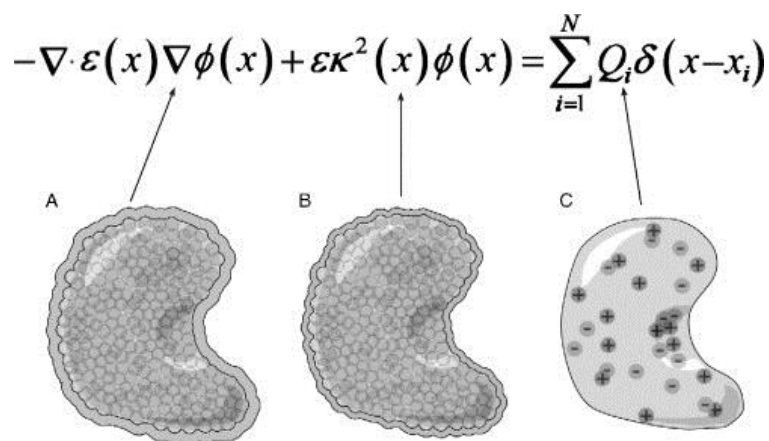
Figure 2.5 A) the dielectric constant is less inside than outside the solute, with small change in the solvent-accessibility surface area. B) The ion-accessibility parameter $\bar{k}^2(x)$ is proportional to the bulk ionic strength outside the ion-accessible solute surface and C) defined point charge at the center of each atom.

CHAPTER III
MATERIALS

3.1 Hardware

- Personal computer (PC)
- Notebook
-High-performance computer cluster "Pheonix" located at Computational Chemistry Unit Cell, Department of Chemistry, Faculty of Science, Chulalongkorn University

3.2 Software

- NAMD 2.7b

A parallel molecular dynamics code designed for high-performance simulation of large biomolecular systems. NAMD was developed by the Theoretical and Computational Biophysics Group in the Beckman Institute for Advanced Science and Technology at the University of Illinois at Urbana-Champaign. The program is distributed free of charge with source code (http://www.ks.uiuc.edu/Research/namd/).

- VMD

A molecular visualization program for displaying, animating, and analyzing large biomolecular systems using 3-D graphics and built-in scripting. VMD was developed by the Theoretical and Computational Biophysics Group in the Beckman Institute for Advanced Science and Technology at the University of Illinois at Urbana-Champaign. The program supports computers running MacOS X, Unix, or Windows, is distributed free of charge, and includes source code (http://www.ks.uiuc.edu/Research/vmd/).

- Wordom

A program for efficient analysis of molecular dynamics simulations. Wordom aims at fast manipulation and analysis of individual molecular structures and

molecular conformation ensembles. The program is used to analyze secondary structure and distance analysis. Wordom is maintained and developed mainly in the Fanelli Lab at the University of Modena and Reggio Emilia (IT). The program is free software under the GPL license (http://wordom.sourceforge.net).

- DSSP

The DSSP (Define Secondary Structure of Proteins)algorithm is the standard method for assigning secondary structure to the amino acids of a protein, given the atomic-resolution coordinates of the protein. The DSSP program was designed by Wolfgang Kabsch and Chris Sander. DSSP is free of charge (http://swift.cmbi.ru.nl/gv/dssp).

- APBS

APBS (Adaptive Poisson-Boltzmann Solver) is a software package for modeling biomolecular solvation through solution of the Poisson-Boltzmann equation (PBE). The program employs one of the most popular continuum models for describing electrostatic interactions between molecular solutes in electrolytic solvent. The program is available with free of charge (http://www.poissonboltzmann.org/apbs).

- APBSmem

A Java-based graphical user interface for Poisson-Boltzmann electrostatics calculations at the membrane. APBSmem enables users to perform electrostatics calculations on biomolecules in an implicit membrane environment. The program is an open source software available with free of charge (http://sourceforge.net/projects/apbsmem).

- PDB2PQR

An automated pipeline for the setup, execution, and analysis of Poisson-Boltzmann electrostatics calculations. PDB2PQR is a Python software package for converting protein files in PDB format to PQR format that can be used in APBS program for continuum electrostatics calculations. The program can be freely obtained after registration at http://kryptonite.nbcr.net/pdb2pqr.

- SSH secure shell:

 SSH client is a secure network connection system which run on local computer, login for secure data communication between 2 network computers, that it connect through secure channel for transfer information between computing cluster and personal computer.

- Scripting commands and input files

 To run or analysis of the programs used in this study, some useful scripting commands used files are provided in appendix.

CHAPTER IV
COMPUTATIONAL STUDY OF UP AND DOWN-STATE
CONFORMATIONS OF KvAP-VOLTAGE SENSOR

4.1 Introduction

Voltage-dependent ion channels sense changes in transmembrane electric fields by the rearrangement of the positively charged residues (predominantly arginines) along the S4 helix in the voltage-sensing domain (VSD). The key significance for the S4 motion is to drive the pore domain to open (activated) or close (resting) the gate of the channels. An activation of voltage-gated potassium channels (K_v) requires zero millivolt of membrane potential, while approximately -70 mV of membrane voltage stabilizes the channels in the resting state. K_v channels are tetramer (Figure 4.1), each consisting of six transmembrane segments (S1–S6). S5-S6 helices of the four chains assemble to form the central pore, which is surrounded by four voltage sensor domains (S1-S4).

The molecular mechanism of voltage-dependent conformational changes of VSD is not clearly understood. Nevertheless, the S4 sensor segment is rich in positively charged arginines. The motion of S4 must, hence, be associated with the movement of the gating charges. There has been extensive debate concerning voltage-sensing conformational changes has resulted in three conceptual models of S4 motion called "Transporter", "Helical screw" and "Paddle" (Figure 1.7). The three models share a common change in the position of the positively charged arginines, by which the S4 helix moves outwardly the membrane during depolarization state (activation). In the resting state, the S4 helix moves toward the membrane interior. According to the positions of the charged arginines on S4, the activated channel with an outward motion of VSD is called "Up" state while the closed channel with an inward motion of VSD is called "Down" state.
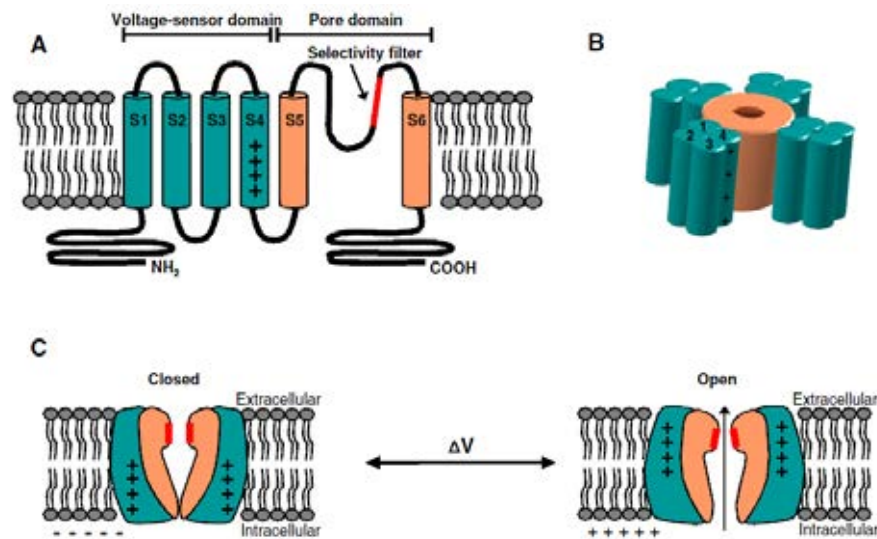
Figure 4.1 The general structure of voltage–gated ion channels. (A) Each domain is consisted of six transmembrane S1–S6. The VSD (green) is a positively charged arginine on S4 at every third position. (B) The PD (orange) form S5-S6 helices that is the region for ions pass through to membrane. And (C)when the changing membrane potential to depolarization state, the S4 helix moves outwardly the membrane and results to the PD open [37].

Unfortunately, crystal structures of a number of voltage-gated ion channels including Kv1.2, KvAP, NavAb and NavRh [68] have only revealed the voltage sensor in the activated or "Up" state conformation because these experiments were carried out in the absence of membrane potential. To understand the molecular mechanism of the movement of S4, detailed structure information of both the "Up" and "Down" conformations of the VSD is essential. High-resolution structure determination of voltage dependence protein systems remains technically challenges but has not been achieved so far. Other approaches that can shift the population of the VSD conformation toward the Down state become an alternative choice of the study.

Amino acid sequence and structural arrangement of transmembrane segments (S1-S4) of KvAP voltage sensor domain in the Up conformation were shown in Figure.4.2. From the x-ray structure (1ORS), the four transmembrane segments of voltage sensor domains arrange in a counter-clockwise direction. Conformational

changes and the role of conserved residues of the VSD for the molecular mechanisms of voltage-dependent function have been extensively addressed by both experimental and theoretical studies. In the S1 segment, Glu45 is a conserved acidic residue found in voltage-gated K^+ and Na^+ channels. It has been proposed that this negatively charged residue may involve in salt-bridge interactions with the positively charged arginines of the S4 segment in the resting state of voltage gated channels [37]. Asp62 on the S2 segment has been reported to play a role in stabilizing the voltage sensor in lipid region by forming a salt-bridge interaction with arginine residues on the S4 segment [40, 69]. The S3 segment is not a continuous helix. Its secondary structure was separated into S3a and S3b. In the S3b helix, Glu107 forms salt-bridge interactions with Arg122 of S4 segment. The S4 helix of KvAP-VSD consists of a series of highly conserved arginines, Arg117, Arg120, Arg123, Arg126 and Arg133 (termed R1, R2, R3, R4 and R6 respectively) [40]. Several evidences suggested the S4 arginine residues move through the electric field within membrane during the channel opening and resting [33, 37]. The protein charge movement through the membrane electric field is known as "the gating charge".

In this chapter, a computational study of Up and Down state conformations of the voltage sensor from the prokaryotic K^+ channel KvAP is presented. Structure models of Down sensor conformation was developed based on spin-labeled EPR data. Molecular dynamics simulations and solvent continuum gating charge calculations of the structure models were carried out to validate the quality of the models.
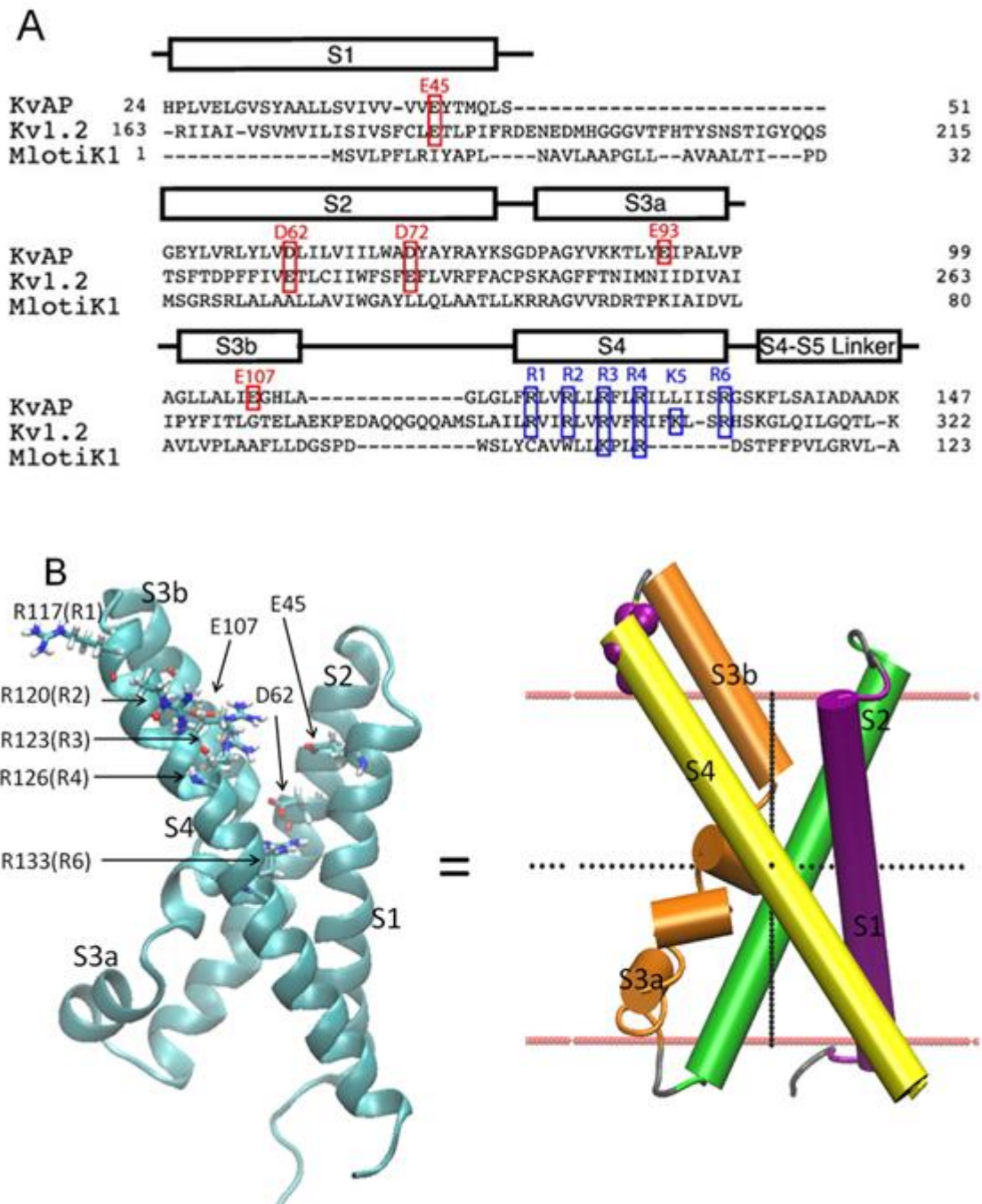
Figure 4.2 (A) Amino acid sequence alignment of voltage-gated KvAP, Kv1.2 and cyclic nucleotide-modulated MlotK1 potassium channels (B) Schematic representation of KvAP voltage sensor domain (S1-S4) along with important conserved residues.

4.2 Computational details

4.2.1 Structure modeling

The Up state conformation of the KvAP-VSD is already available from the crystal structure (PDB code:1ORS). A structure model of KvAP-voltage sensor in a down state was taken from the Perozo's work [70]. This structure was built using pseudoatom driven solvent accessibility refinement (PaDSAR) approach [70-71]. The PaDSAR structure calculation employed restrained molecular dynamics (RMD) using distance and solvent accessibility data derived from experimental EPR technique as structural restraints (Figure 4.3). Detailed information for the PaDSAR approach has been published previously [71]. Although the Down sensor conformation of KvAP was obtained from the previous work, a structure modeling methodology is concisely provided. A strategy for the structure calculation of the down conformation is described briefly in the next paragraph.
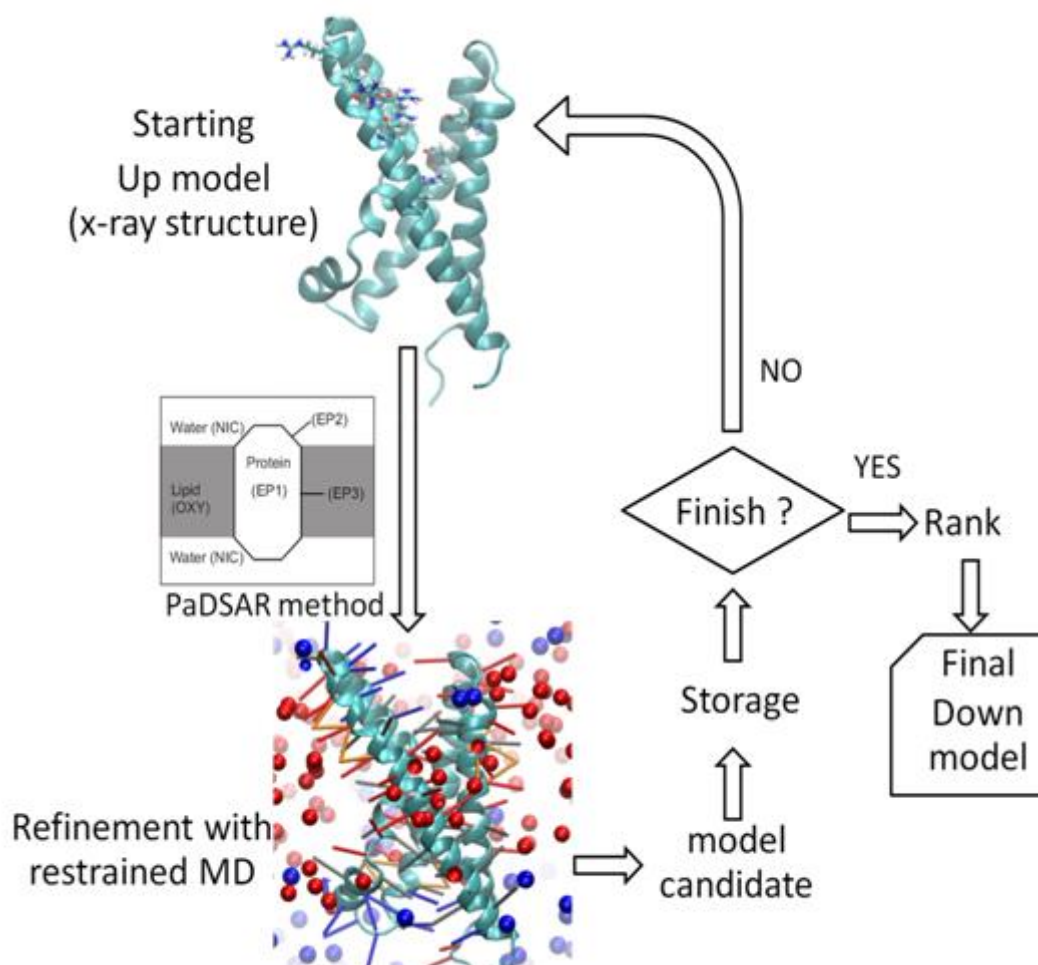
Figure 4.3 Schematic methodology of structure refinement of Down-state model using restrained molecular dynamics calculation (PaDSAR method). The experimentally-derived restraints were from spin-labeled EPR data provided by Perozo et al [73].

In the first step, the KvAP-VSD crystal structure (1ORS) representing the voltage sensor conformation in the Up-state was used as a starting structure. A set of distance and accessibility restraints obtained from spin labeled protein samples determined in a specially designed lipid bilayer called dioleoyltrimethylammonium-propane (DOTAP) were introduced as the PaDSAR restraints to enforce the Up-state conformation towards conformations of the Down-state. This type of lipids has been shown to be able to shift the population of voltage sensor from the Up to Down states

via protein-ligand interactions [72]. The PaDSAR method was incorporated in the CHARMM program version c32a2. In the PaDSAR method, each residue of the protein was subjected to attach with two virtual particles, backbone and the pre-assigned spin-probe pseudoatoms (EP1 = buried, EP2 = water exposure and EP3 = lipid exposure). During the course of molecular dynamics (MD) calculations, restraint driving forces to spin-probe particles were governed by interactions with environment pseudoatoms, backbone, O_2 (OXY) and NiEdda (NIC).The VSD was modeled with all heavy atoms and all polar hydrogens with the extended-atom PARAM19 force field. The structure calculation was performed with several cycles of PaDSAR runs. Structures that gave an excellent agreement with experimental data were selected as a potential Down-state model. The reliability of models were further examined by molecular dynamics simulations and gating charge calculations.

4.2.2 Molecular dynamics simulations

Molecular models of KvAP-VSD consisting of a model of the Up state and two models of the Down state were embedded in a POPC (palmitoyloleoyl-phosphatidylcholines) bilayer and TIP3P waters. Side-chain ionization states that were expected at pH 7 were assigned based on pK_a calculations using PROPKA. Sodium and chloride counterions were added to neutralize charges on the system using VMD's Autoionize plugin.

Preparation protocol of the model system for the simulation of protein in lipid bilayer was shown in Figure 4.4. First, the optimal position of protein in membrane was determined using Poisson-Boltzmann free energy calculation of membrane solvation (describe in the next chapter). Next, the oriented protein was solvated with a 3 Å layer of water using the SOLVATE program. Then water molecules located within the bilayer region were removed. After that, the resulting structure was embedded in a pre-equilibrated and hydrated POPC lipid bilayer. In this step, all lipid molecules, of which the positions overlapped with the protein, were deleted, along with all water molecules the overlapped with the lipid bilayer. In this final preparation step, water and Na^+ and Cl^- were added to the system to make a cuboid shape of $\sim 80 \times 80 \times 80$ Å^3.
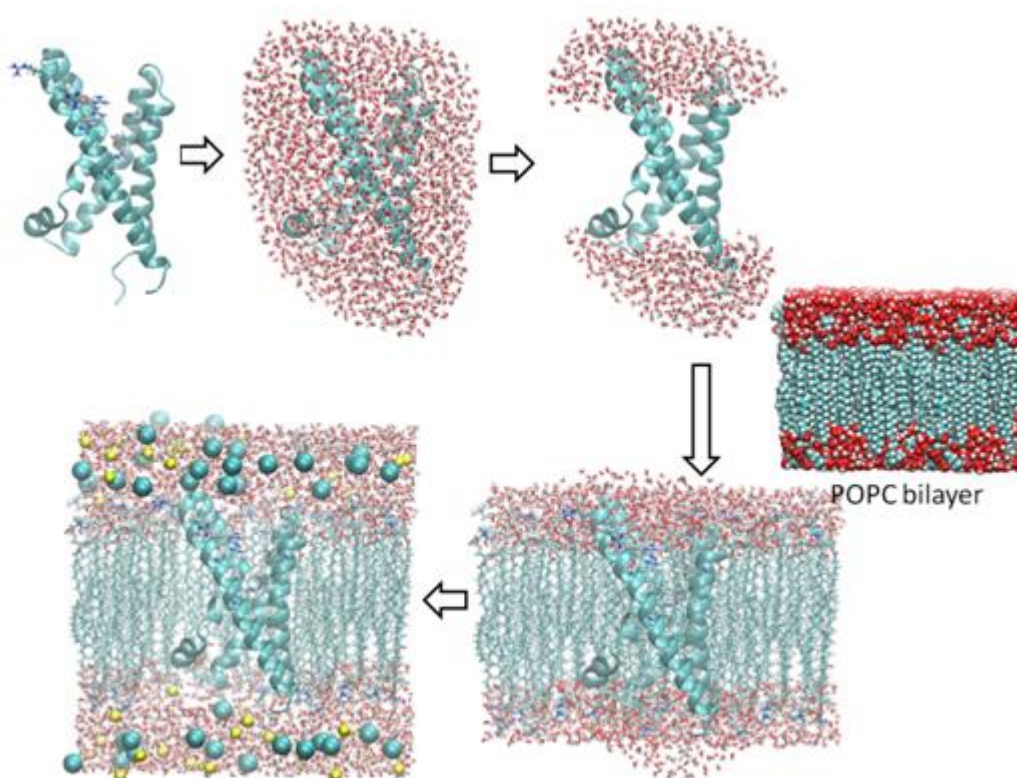
Figure 4.4 Methodology flowchart for preparing the model system for the simulation of protein in POPC lipid bilayer.

Four atomistic simulations the proteins in hydrated POPC bilayer were carried out using NAMD2.8b2, a free-of-charge molecular dynamics simulation package. The CHARMM force field parameters are CHARMM 22 for protein and CHARMM 27 for lipid molecules. The TIP3P water potential was employed in simulations. To reduce finite-size effects, periodic boundary conditions were used in molecular dynamics simulations with a periodic dimension of 79 x 78 x 81 Å^3. The calculation of long-range electrostatic interactions in periodic membrane-protein system employed the particle mesh Ewald summation method. A distance cut-off of 12 Å was used for calculating short-range non-bonded interactions. SHAKE and SETTLE algorithms were used for keeping the bond between each hydrogen and the heavy atom to which it is attached at fixed distance. The simulations were performed at constant pressure of 1 atm and constant temperature of 298 K. Langevin dynamics (LD) was used for controlling the temperature of the system and the system was controlled the pressure by using a Nośe-Hoove Langevin Piston.

Energy minimizations and restrained MD simulations were employed to relax geometric, angle, torsional and other structural strains of the model systems. During the first restrained MD run, atoms for protein and lipid head groups were restrained to their initial positions using the harmonic potential function. In the subsequent run, protein atoms were restrained, leaving the rest of the system to be relaxed. Finally, all positional restraints were removed and an equilibration run was performed.50 ns MD simulations were performed for each system with the time step of 2 fs.
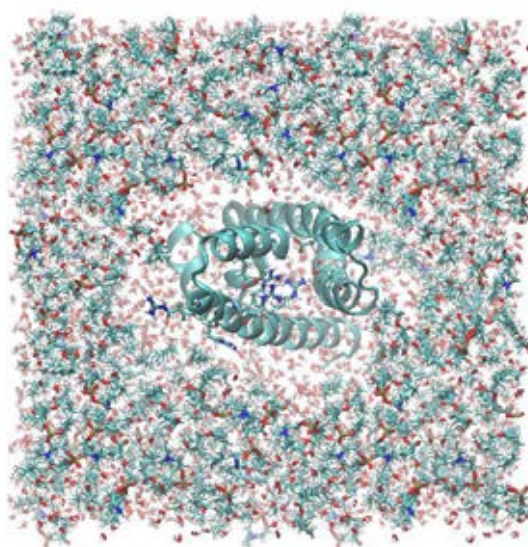
Figure 4.5 Extracellular side (top view) of model system of KvAP-VSD in hydrated POPC bilayer

4.2.3 Analysis of MD trajectory

The results of all MD simulations were analyzed including root-mean square deviation (RMSD), inter-helical salt-bridge interactions (hydrogen bonding) profile of S4 arginines, secondary structure element and solvent density profile. RMSD was computed using VMD scripts modified for the studied systems. Analysis of salt-bridge interactions and secondary structures were done using the program WORDOM, python scripts and gnuplot. Salt-bridge interactions involving arginine side chain were analyzed on the basis of hydrogen bonding geometry, in which a

distance between the guanidinium donor group of arginines and the carboxylate acceptor group of glutamate or aspartate residues. Secondary structure element of protein structure was characterized based on DSSP criteria. Plots of solvent density profile were obtained using VMD plugin. Unless otherwise stated, 20 ns duration of production run were used for trajectory analysis. Graphical representation of protein structures and membrane-protein systems was primarily obtained using the VMD program.

4.2.4 Modeling membrane potential in molecular dynamics

The simulations of KvAP-VSD in the Down state were carried out and without external membrane potential. Treatment of the membrane potential in MD simulations consists of introducing an external constant electric field (E) perpendicular to the membrane [73]. The applied electric field is calculated by

$$E_z = -V / l_z \tag{4.1}$$

Where V is the applied membrane potential and l_z is the size of the system along the z-axis. The electric field unit in NAMD is kcal/(mol Å e), that is 1 kcal/(mole *A *e) equal to 4.35×10^8 V/M. The appropriate conversion factor for V in volt and l in Å is 23.060549. That is,

$$E_z(kcal\frac{kcal}{mol\ Å\ e}) = -23.060549\frac{V\ (volt)}{l_z\ (Å)} \tag{4.2}$$

The value of l_z is obtained from the c_z value of the NAMD extended system configuration file (the xsc file). The study examined potential differences along the z-axis in a range of -300-300 mV.

Four molecular dynamics runs include a model of the Up state, three models of the Down state. Detailed information of the MD simulation were summarized in Table 4.1.

Table 4.1 Summary of Detailed Molecular Dynamics Simulations

Systems	Models	Electrical field (mV)	Number of solute atoms	Number of water atoms	Number of phospholipid atoms	Total number of atoms
Run1	Up	No	2146	21075	17420	40722
Run2	Down1	No	2146	20973	17152	40352
Run3	Down1$_{ef}$	-70	2146	20973	17152	40352
Run4	Down2$_{ef}$	-70	2146	21132	17286	40645

4.3 Results & Discussion

4.3.1 Model candidates for the KvAP-VSD Down conformation

The structure model of KvAP-VSD used in the study is composed of residues starting from Asp20 to Arg151. The obtained models representing a Down-state conformation of KvAP-VSD were illustrated in Fig. 4.6. The top ten structures were selected based on the best fit with the experimental EPR data. For all the selected models, transmembrane voltage sensor segments undergo a conformational change that is similar but different in magnitude. The most significant conformation drift was found in S1, S3b and S4 helices. The S2 and S3a helices remain almost unchanged. By comparing with the Up conformation, the outer end (top part) of S3b and S4 helices rotate downward (inward translation) in the membrane interior. The predominant motion of KvAP voltage sensor domain appears to be a tilt-and-slide of the S4 helix. A substantial movement of the S3b helix was also observed because this part is connected with the S4 helix.
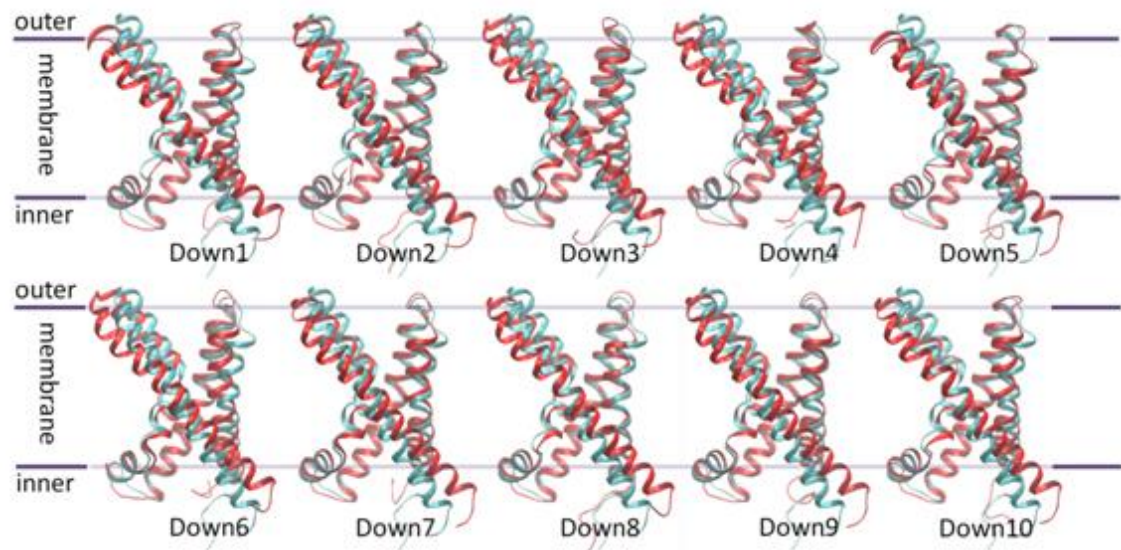
Figure 4.6 The best ten structure models of KvAP-VSD Down state conformation. Down model is shown in red color and Up model is shown in cyan color.

Comparison of the structures of Up to Down models suggested S4 undergoes a tilt of the helix along with a slight rotation about its helical axis (Fig 4.7). This makes the S4-top, especially the gating charge arginines, inserted deeply into the hydrophobic membrane. As a result, several side chains of S4 arginines rearrange in a way to avoid unfavorable interactions between the charge arginines and hydrophobic groups of the lipid tails. For instance, the first Arg117 (R1) side chain of the Up model exposed to water-lipid interface. In the Down model, Arg117 was positioned deeply inside the hydrophobic membrane, and possibly interacts with phosphate group of the lipid. Interactions between the Arg117 side chain and hydrophobic tails of the lipid would be unfavorable. To overcome such circumstances, Arg117 may to need straight its side chain toward lipid-water interface. From the structure comparison, it was found that the Arg120 (R2) side chain, which partially exposed to the lipid in the Up state, was buried inside into the VSD core due to a slight S4 rotation. Effects of the S4 displacement led to an exchange of salt-bridge interactions of Arg123 (R3)-Glu107. The interactions were changed to Arg123 (R3)-Glu45 and to Arg120 (R2)-Glu107 when the channel switches from the activated to the resting states. Mode of S4 motion is clearly illustrated in Figure 4.7.
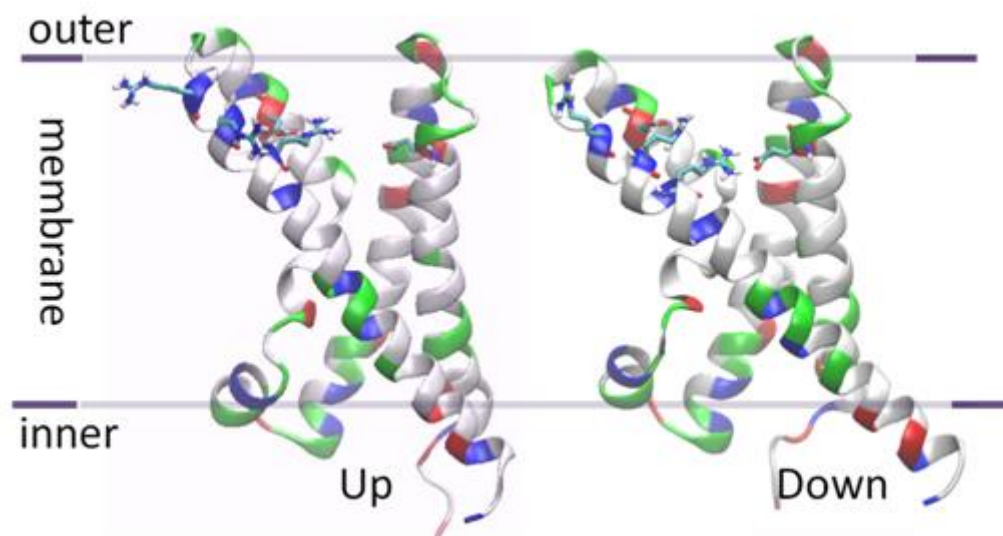
Figure 4.7 Comparison of structure models between the Up and Down conformations suggesting the S4 displacement corresponding to tilt and shift mechanism

4.3.2 Optimal position of KvAP-VSD in membrane

Several evidences showed that improper arrangement of proteins in membrane could produce structural instability of simulated systems due to the effect of hydrophobic mismatch. This problem was addressed by performing a computational search method to guide the optimal spatial position of proteins in membrane prior to MD simulation. In this study, a total of 20 structure configurations of KvAP-VSD were generated by translating the VSD structure along the z-axis in a range of -9 Å to +10 Å from the membrane center (the origin). Each configuration was separated with the distance of 1 Å. The relative electrostatic free energy ($\Delta\Delta G_{elec}$) of membrane solvation computed by the Poisson-Boltzmann solvent continuum method was shown in Figure 4.8. From the results, more VSD was immersed within the membrane, the lower the energetic cost was obtained. The lowest value of the $\Delta\Delta G_{elec}$ plot corresponds to the configuration, of which the VSD center of mass lies about 2.0 Å away from the membrane center in the intracellular side. This configuration was considered as the optimal position. In this configuration, all the four transmembrane

segments sit nicely within the membrane region. The results agree well with the typical position of transmembrane segments used in MD simulations [74].
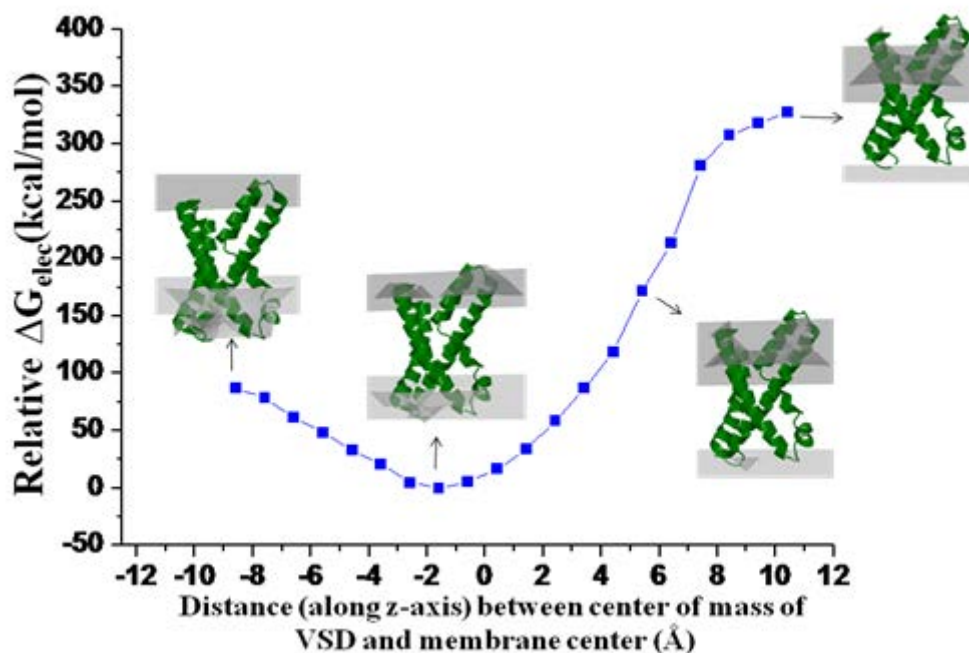
Figure 4.8 Relative free energy of solvation of KvAP-VSD inserted into membrane at different penetration depth.

4.3.3 Structure and dynamics of KvAP-VSD from MD simulations

50 ns all atom MD simulations of four model systems were performed in an explicit solvent environment. The RMSD plots as a function of simulation time was shown in Figure 4.9.From the results, small RMSD values in the beginning of the simulation time were due to constraints imposed on the protein backbone. RMSD increases when removing the position constraints. The production phase can be considered after 30 ns of the simulation time. In this phase, the backbone RMSD fluctuated in a range of 1.5-3 Å compared with the starting structure. An overall RMSD profile indicates a stability of structural and dynamical properties of the four simulation systems.
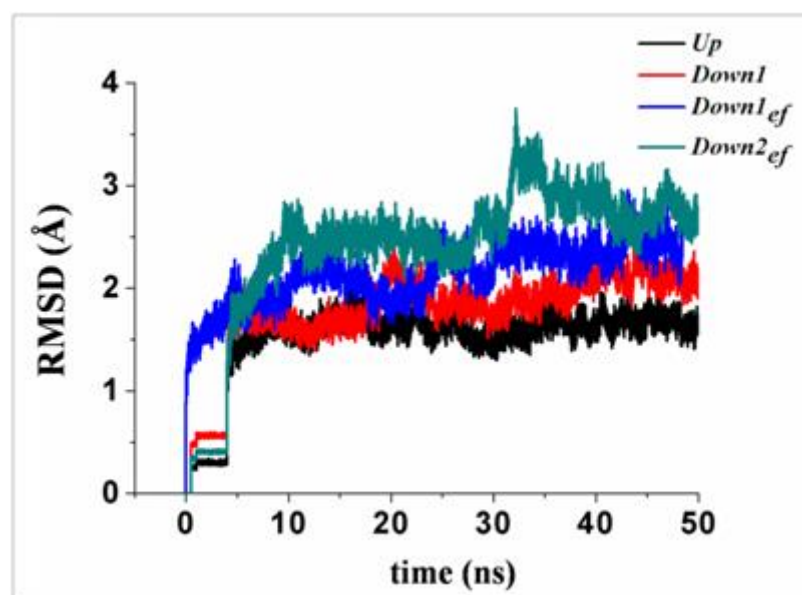
Figure 4.9 VSD structure is stable with backbone RMSD of 1.5-3.0±0.5 Å of all four systems with respect to the starting structure.

Structural dynamics of each transmembrane helix of KvAP-VSD were evaluated from MD trajectories of the four systems (Fig. 4.10). An overall view of RMSD profiles of all simulated systems indicates the transmembrane S1-S4 helices fluctuate considerably with the range of RMSD values between 1.0 and 2.0 Å. This suggested structural stability of the segments during the course of MD simulations.

The fluctuation profile of RMSD for the Up model appears to be a common pattern for the simulation of VSD in the absence of membrane potential. This is because the VSD of the voltage-gated channels is greatly stabilized at the zero voltage. A challenge study is one in which the simulations of the Down models were carried out with and without membrane voltage. A surprising result was found for Down1, of which the simulation was carried out without membrane potential. A RMSD profile of the S4 helix of Down1 shows a small fluctuation, implying structural stability of the sensor segment in the lipid bilayer. In contrast with a previous report, the simulation of the Down-state model of Na_v voltage sensor showed a deformation of the secondary structure of the S4 helix because no membrane potential term has been applied.
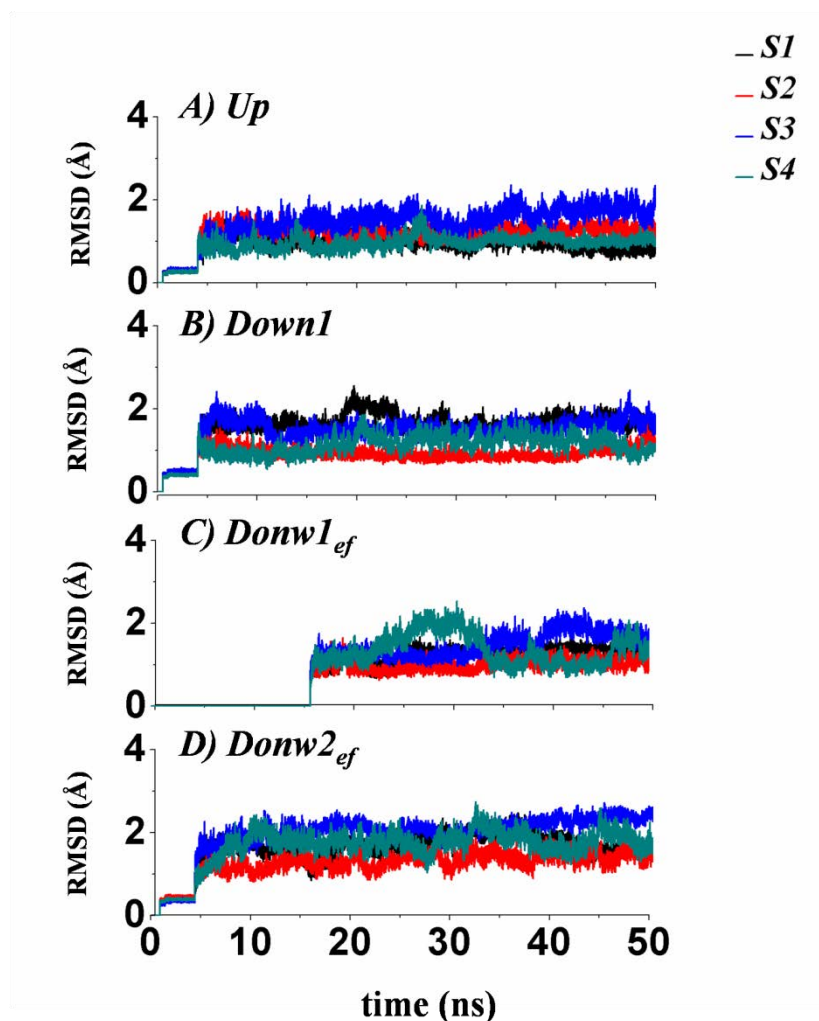
Figure 4.10 RMSD of individual TM segment (S1-S4) of all four MD systems as a function of simulation time**.**

4.3.4 Stability of helical transmembrane segments

To further validate stability of helical secondary structure, the backbone conformations of all structure models in the MD trajectories were analyzed. Graphical representations of secondary structure analysis obtained from structures in the MD trajectories were shown in Figure 4.11. From the plots, helical structures of the voltage sensor segments (S1-S4) in the four simulations were mostly maintained during the simulations. Especially, the Up model shows no significant disruption of all S1-S4 helices. For the simulations without membrane potential (Down1), the S1 helix begins to break (two black regions around positions 25 to 30 and 43 to 45) after

5ns of the simulation. However, the plot of helix break is not continuous, indicating that the helical deformation is a temporary event. The simulations with membrane potential (Down1ef and Down2ef) revealed a similar behavior of helical stability of the voltage sensor segments, except for S1. A continuous red and smooth band of the S1 helix was observed for positions 43 to 45, suggesting stable helical conformation. An obvious break of the S1 helix was shown for positions 25 to 30 (a long black band). However, the nature of helical breaking of the S1 helix remains unclear.
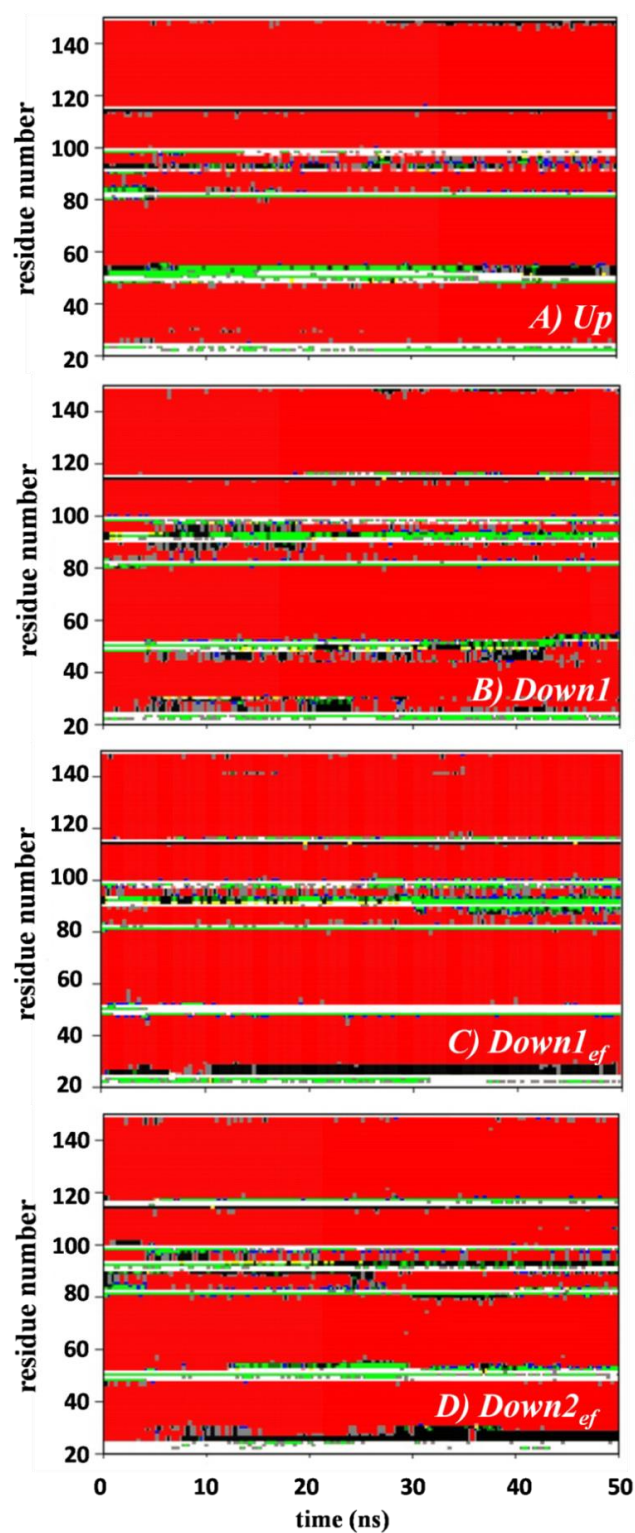
Figure 4.11 The secondary structure of KvAP-VSD as a function of simulation time, each color indicate: α-helix (red), β-bridge (yellow), stand in β sheet (blue), β-turn (black), coil (green), unassigned (white)**.** Types of secondary structures were identified based on DSSP algorithm.

4.3.5 Salt bridge interaction

Salt-bridge interactions between the positive charge arginines on the S4 helix and the negative charge glutamate or aspartate residues located on S1, S2, S3a and S3b helices were analyzed on the basis of hydrogen bonding interactions. The gating charge arginines are located at every third position on S4, and surrounded by the lipid environment and residues of other transmembrane segments. One should expect that the motion of the S4 sensor would change the countercharge interactions with the neighbored environment. Hydrogen bond distances involving S4 arginines include R117(R1), R120(R2), R123(R3), R126(R4) and R133(R6) were analyzed from the four MD trajectories. The results are illustrated in Figure 4.12.

The simulation of the Up conformation revealed that three salt-bridge pairs involving R123, R126 and R133, can be defined. From the distance profiles, the guanidinium group of R123 forms a stable salt bridge with E107 whereas the R133 side chain was placed closely with D62 during the last 10 ns of the simulation. In addition, the R126 side chain might participate in salt bridge with E107 (Figure 4.12). The other two arginines, R117 and R120 are water-lipid exposed and thus, do not engage in salt bridge interactions. A hydrogen-bonded network of water and lipid phosphate headgroups formed around the guanidinium groups of R117 and R120 was found instead. A number of studies suggested that interactions between the charged residues of the VSD and the lipid phosphate groups are necessary for the stability and function of Kv channels.

An apparent change in distance-based salt bridge patterns was observed for the simulation of Down1, Down1ef and Down2ef (Figure 4.12). The different patterns suggested changes of the gating charge environment. The simulations suggested that salt-bridge interaction between R133 and D62 was observed in Down1 and Down1ef. However, this salt-bridge pair was changed to R133-E93 in Down2ef. For R126, a salt-bridge formation with E107 observed in the Up conformation was also preferable in the Down1 and Down1ef, but no longer detected in Down2ef. A favorable salt-bridge formation of R123-E127 can be defined in Up, Down1 and Down1ef. In Down2ef, residues making this salt-bridge pair were changed to R123-E45. In addition, the simulation of Down2ef revealed a new salt-bridge formed by R120-

E107. This R120 was not involved in salt-bridge interaction in the simulation of Up state. For the overall comparison, it appears that salt-bridge interacting pattern observed in the simulations of Down1 and Down1ef were similar to that of Up simulation. The most difference in salt-bridge pattern was found from the Down2ef simulation.
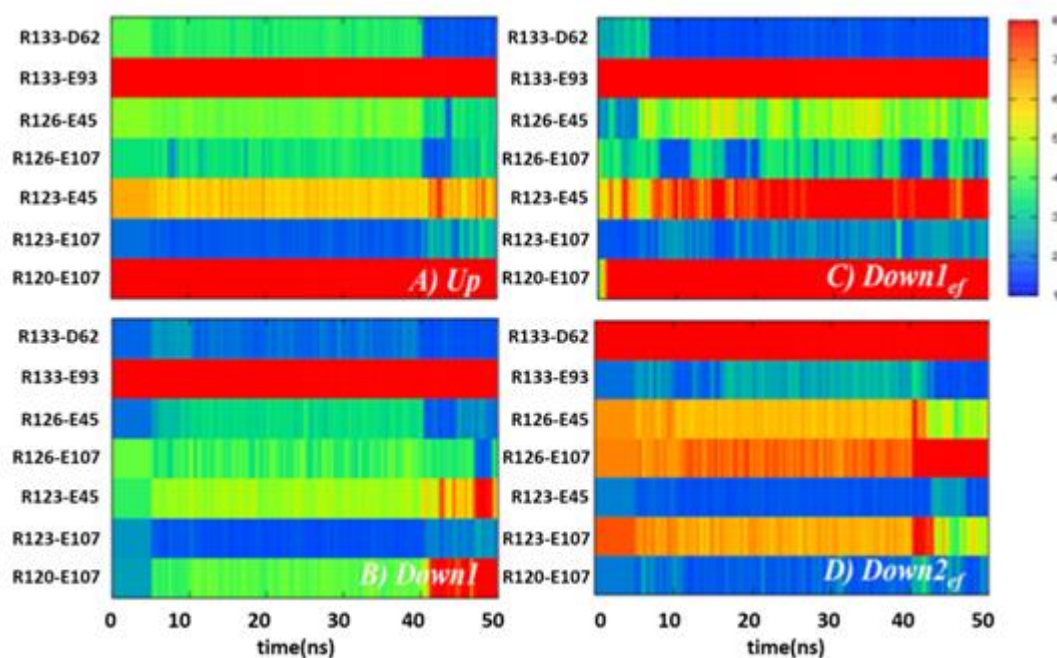
Figure 4.12 Color scale represents the distance of salt-bridge interactions in KvAP-VSD consistent with x-ray data.
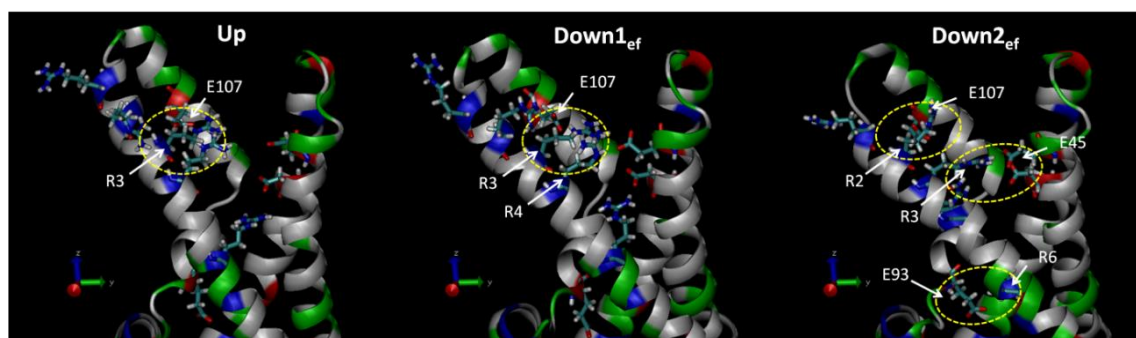
Figure 4.13 Represent salt-bridge interaction between charge residues on KvAP-VSD of Up and Down model

4.3.6 Water-filled crevices in the VSD core

There has been strong evidence that the arrangement of the four segments of the VSD creates water-filled crevices, where water molecules can penetrate into the membrane. The crevices have hourglass shape structure as the VSD helices tilted against each other (Figure 4.13). In all the simulations, water molecules diffuse from both extracellular and intracellular solution into the empty crevice forming a narrow water-filled pore near the center of the S1–S4 helical bundle. The narrowest constriction region controls an amount of water molecules accessible into the crevices. Because the polarity of waters increases the local dielectric within the bilayer, the presence of water in the VSD core was expected to maintain the charged arginine side chains in the membrane by lowering the hydrophobic barrier.
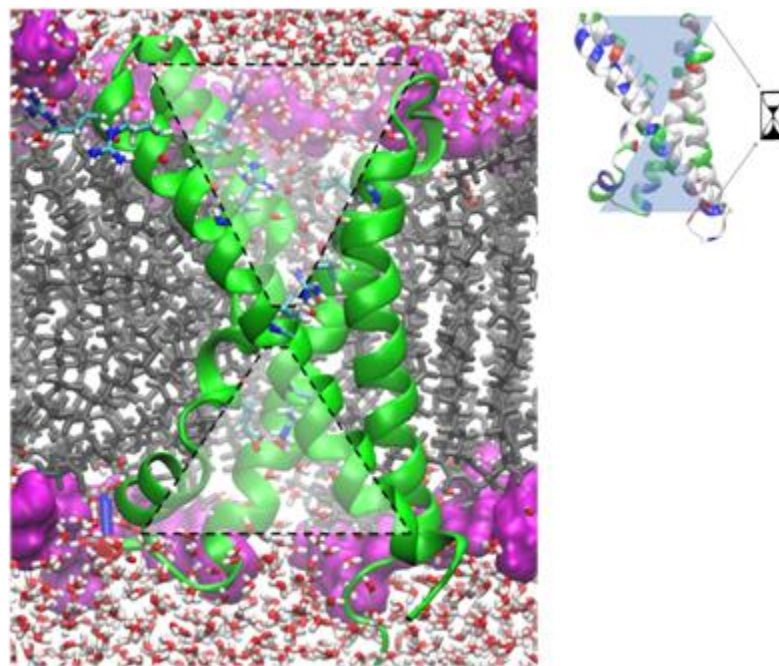
Figure 4.14 The hourglass-like feature of the VSD revealed two cavities that allow the water molecules solvated the charge residues innermembrane.
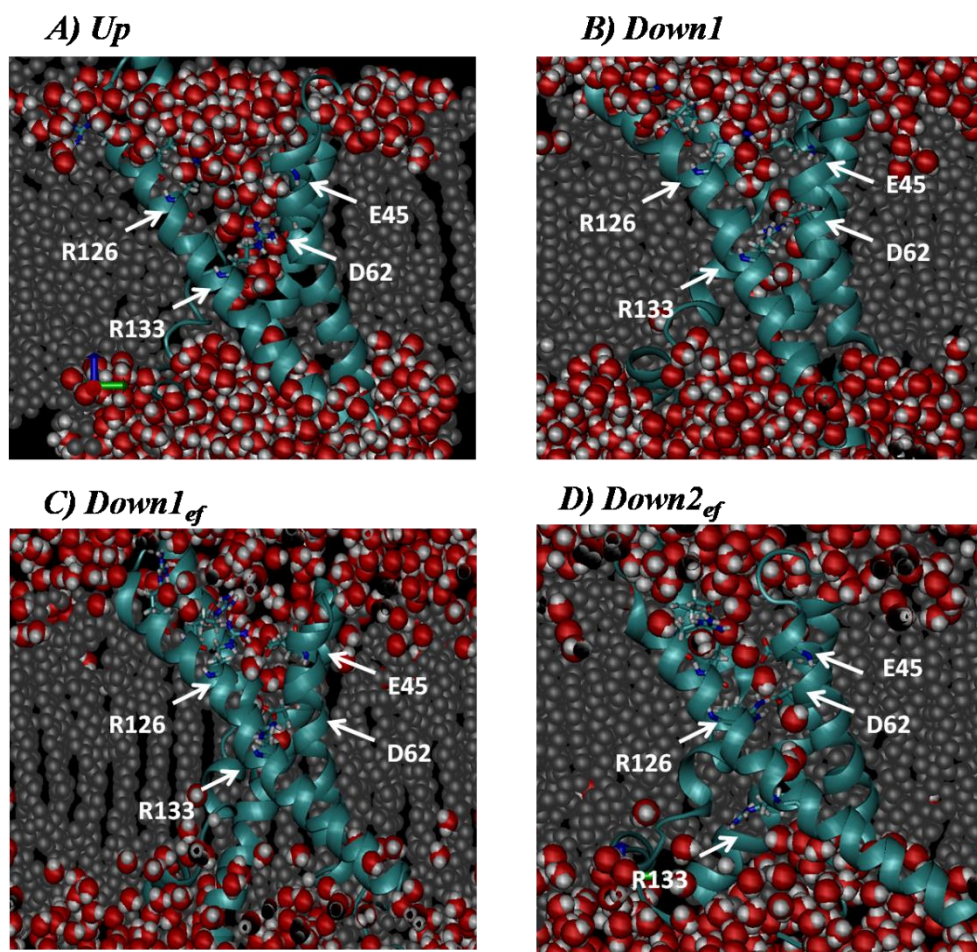
Figure 4.15 Water-filled crevices on KvAP-VSD

4.3.7 Water distribution and the position of S4 arginines in the VSD

A further analysis has focused on the density profiles of water, lipid and S4 arginines in membrane (Figure 4.15). These density profiles were computed over the last 15 ns of the simulation. The density profiles shown in figure insets suggested that in membrane region there is a very low content of water (red color), but high lipid content (black color). This distribution pattern of solvent density is commonly found MD simulations of membrane protein systems. Magnifying these graph highlighted the presence of waters in the lipid bilayer. This result supports water penetration into the hydrophobic region of the lipid bilayer and the presence of water-filled crevice of voltage sensor domain.

An interesting property that can be extracted from these plots has focused on the movement of the S4 arginines between Up and Down states. The simulation of Up state showed that R117 and R120 are near water-lipid interface whilst R123, R126 and R133 are more deep inside hydrophobic region of the lipid bilayer. From the density profiles of Down1 and Down1ef, the distribution of these five arginines positions in overall slightly shifted with respect to that of the Up simulation, and that allows the S4 segment to move toward the lipid bilayer with an average distance of 2Å relative to the membrane normal (Table 4.2). The magnitude of this movement is small compared to that observed in Down2ef, with which the distance displacement is about 5Å relative to the membrane normal. The magnitude of the displacement has transferred all five arginines into lipid bilayer.
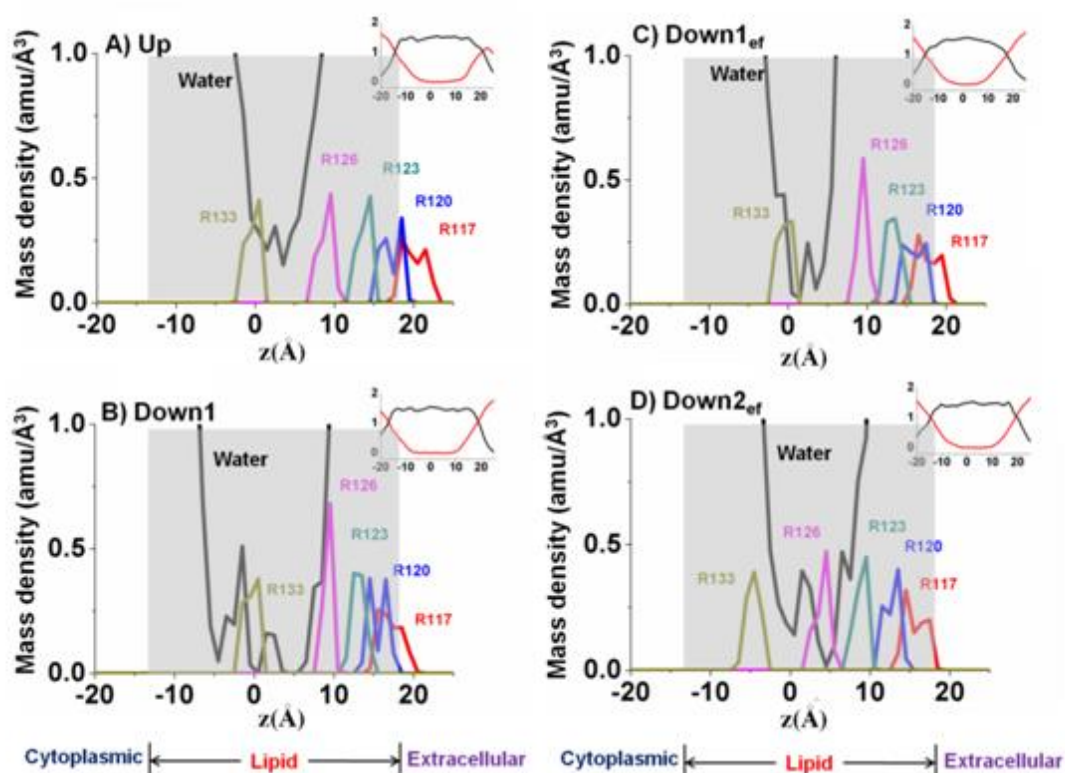
Figure 4.16 Density profile, comparing the distribution of water (back), lipids (red), and the four arginines in simulations of the up and down states. The densities were averaged over the last 15 ns.

Table 4.2 Average distance displacement of S4 arginines computed from the last 15 ns of MD trajectory.

ΔZ / Residue	Up-Down1(Å)	Up-Down1ef(Å)	Up-Down2ef(Å)
R117(R1)	2.5±3.0	2.0±2.5	4.0±2.5
R120(R2)	2.0±2.0	1.5±2.5	5.0±2.0
R123(R3)	0.5±1.5	0.5±1.5	4.5±1.5
R126(R4)	-0.5±1.0	0.0±1.5	5.0±1.5
R133(R6)	-0.5±1.0	-0.5±1.0	4.0±1.5

4.3.8 Gating charge calculation

At 0 mV the VSD conformation is most populated in the "Up" or depolarization state (also called activated or open) whereas the "Down" or the hyperpolarization state (also called resting or closed) is stabilized around -70 mV. It has been known that the S4 of VSD responses to change in membrane potential by undergoing conformational changes. As the membrane potential changes, the charged arginines on S4 experience a driving force due to the electric field across the membrane. A quantity of electric charge moving across the membrane under the influence of membrane electric field is known as the ''gating charge'' that is defined as the fraction of the membrane electric field traversed by charges on the protein during the gating process. Continuum electrostatic calculations to determine the gating charge in the presence of the transmembrane potential has been previously reported [38].

In this study, the gating charge calculation was carried out to validate the Down models. For representative structures of the gating motion, the "Up"

conformation was used as the starting state and the Down conformation is represented the final state. Atomic charges and radii of the proteins were assigned using the PDB2PQR software. The gating charge calculations were carried out with three levels of focusing from a cubic system of $300 \times 300 \times 300$ Å^3 for coarse, $120 \times 120 \times 120$ Å^3 for medium, and $60 \times 60 \times 60$ Å^3 for fine resolutions. Multi-slab dielectric of the implicit solvent was introduced with the dielectric constants $\varepsilon_m = 2$ for the membrane and $\varepsilon_w = 80$ for water models (Figure 4.16). A thickness of membrane slab was 20 Å. The bathing solution contains ionic strength of 0.1 M with coulomb charge +1 and -1, and radius 2.0 Å.
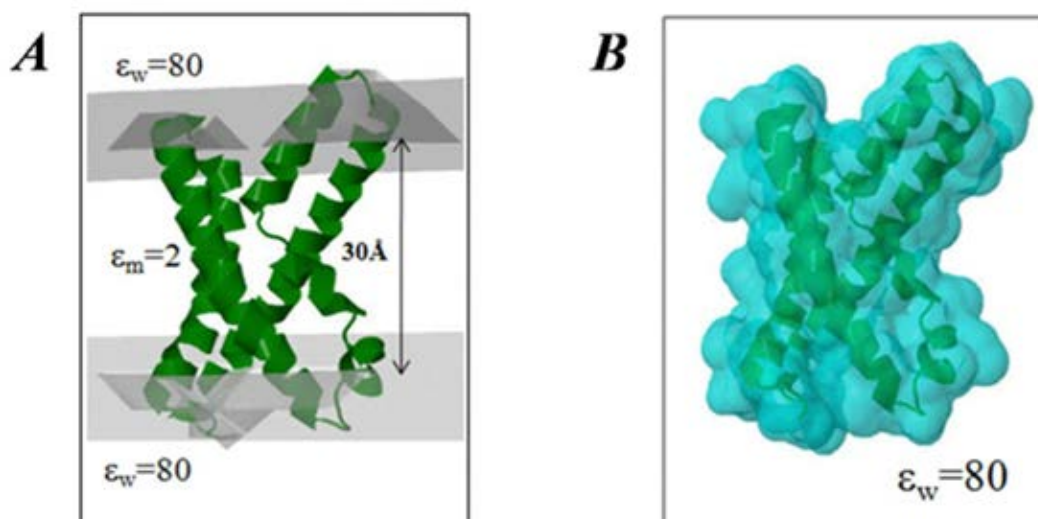
Figure 4.17 Schematic represent structure model for gating charge calculation A) the VSD is embedded in the membrane with discrete dielectric coefficient among inhomogeneous phase while B) the VSD is solvated by water with homogeneous surrounding.

The membrane potential of the inner bath varies from +75 mV to -75 mV while the potential of the outer bath was kept at 0 mV (Figure 4.17).Water probe radius was 1.4 Å. The linearized PB equation was employed to solve using focused boundary conditions at 298.15 K. The calculations were performed by using the program Adaptive Poisson-Boltzmann Solver (APBS) 1.2.1 [75] with help of a java-

based graphical user interface APBSmem for setting up input parameters [59].All the parameters used for this case study are summarized in Table 4.3.
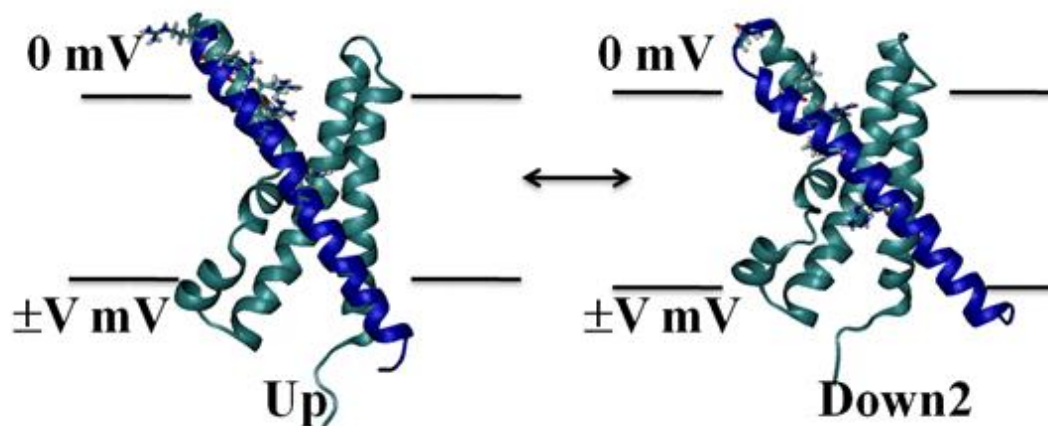
Figure 4.18 The membrane potential contribution to the energy difference due to the VSD motion from the Up to Down2 of gating charge calculation

Table 4.3 Parameters for gating charge calculation

Parameter	Value
Coarse Grid Lengths	300 x 300 x 300
Medium Grid Lengths	120 x 120 x 120
Fine Drid Lengths	60 x 60 x 60
Grid Dimensions	161 x 161 x 161
Counter-Ions	1.0, 0.10, 2.0
Protein Dielectric	2.0
Solvent Dilectric	80.0
Membrane Dielectric	2.0
Headgroup Dielectric	80.0
Solution Method	lpbe
Membrane potential -75 to +75 mV	
Solvent probe radius (srad)	1.4
Temperature	298.15
Z-position of membrane bottom	-10
Membrane thickness	20
Headgroup thickness	0
Upper exclusion radius	18.5
Lower exclusion radius	18.5

The curve of the energy difference versus voltage dependence was shown in Figure 4.18. The results of the gating charge calculation illustrate the membrane potential's contribution to the energy difference due to the VSD motion from the Up to Down1 and to Down2 using the starting MD configurations (Figure 4.17). The energy difference due to interaction of the VSD charges experiencing the membrane electric field at -75 mV was about -9 kT for Up-Down1 and -15 kT for Up-Down2. The energy difference increases as the membrane potential increases. The gating charge obtained from the slope of voltage dependence curve is 1.7e for Down1 and 2.8e for Down2.

Gating Charge Results
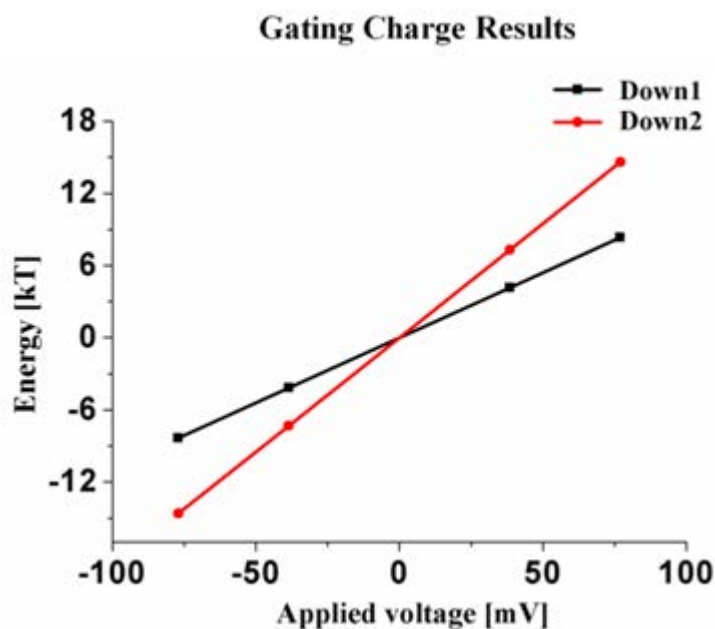
The results of the gating charge calculation using a total of 12 MD snapshot structures of Down1, Down1ef and Down2ef was summarized in Table 4. The gating charge of voltage-gated potassium channel reported by both experimental and theoretical studies was about 12-13e for tetrameric channel which is equivalent to ~3 e per monomer. In this study, the Down2 model appears to give the gating charge value (~2.8 e) in good agreement with those reports.

Table 4.4 Gating charge calculation using models from MD simulations

Snapshot	Gating charge(e)		
	Down1	Down1*ef*	Down2*ef*
1	1.6832	1.6832	2.8462
2	1.5916	1.5300	2.8933
3	1.5671	1.7472	2.9478
4	1.6273	1.7137	2.8783
5	1.5334	1.9246	2.8083
6	1.5593	1.8166	2.7859
7	1.5720	1.7925	2.8271
8	1.5944	1.7475	2.8997
9	1.5945	1.7573	2.8896
10	1.5104	1.7520	2.7072
11	1.5043	1.7619	2.6678
12	1.5871	1.6342	2.6862
Average	1.5771	1.7434	2.8198

CHAPTER V

EVALUATION OF TRANSMEMBRANE PROTEIN

POSITION IN OPM DATABASE USING

CONTINUUM ELECTROSTATIC APPROACH

5.1 Introduction

Membrane proteins play important roles in many biological processes, such as cell communication, signal transduction and regulation, cell adhesion and catalysis. They comprise of three categories, integral, peripheral and lipid-anchored proteins, which constitute about one-third of the proteins encoded in the genome. Integral membrane proteins, the major class of membrane proteins, have single or multiple polypeptide segments spanning throughout the lipid bilayer. Secondary and tertiary structures, orientation and packing of transmembrane domain provide key structural features of these proteins to satisfy interactions with the hydrophobic environment of the lipid bilayer at the minimum cost of the solvation free energy.

X-ray protein crystallography is one of the most powerful tools to determine the three-dimension structure and to provide a basis for understanding how proteins perform function at the atomic level. During the past decade, there has been a significant progress in solving high-resolution structures of transmembrane proteins. However, these crystallographic data are in general lack of atomic coordinates of solvent. In other word, the 3D structure of integral membrane proteins alone does not contain precise orientation of transmembrane domain in the lipid bilayer. Unlike water, the head and tail groups of phospholipid bilayer have its own favorable arrangement and interactions to different parts of proteins by providing naturally hydrophilic and hydrophobic constraints. Thus, molecular dynamics (MD) simulation has been extensively employed to extend structure information as well as the solvation of the know x-ray protein structures, giving insight into structure-function relationship. To perform MD simulation of membrane protein systems, there is, however, a need to make several guesses during setting up a proper orientation of protein in phospholipid bilayer as a starting configuration. Consequently, a well-

defined position of transmembrane segments in membrane bilayer is important for stability and reliability of MD trajectory.

Solvent continuum method is one of the most useful tools for estimating free energy of binding/solvation in chemical and biological systems. The method has been shown to be useful for determining the orientation of proteins in membrane. In such method, aqueous solvent is implicitly described by using a high dielectric continuum model while an implicit membrane model is represented by low-dielectric slab. The solute protein is placed in the two solvent environments with a variety of spatial orientations. The difference in the transfer free energy from an aqueous medium to a water-membrane-water is computed for each orientation. The optimal position is obtained on the basis of the minimum energy that costs for the protein transferring between the two media. Calculation of electrostatic contribution to the solvation free energy of the protein can be carried out by solving the Poisson-Boltzmann (PB) theory.

In this study, the use of Poisson-Boltzmann solvent continuum method for positioning proteins in membrane was examined. As described above, the strategy is to calculate the different free energy of solvation for the tested proteins immerged in two solvent media (water and water-lipid) presented by high (for water) and low (for membrane) continuum dielectric slabs. Membrane protein structures were taken from Orientations of Proteins in Membranes (OPM) database (http://opm.phar.umich.edu/) for the study.OPM database is a collection of transmembrane and membrane-associated proteins, whose structures are pre-oriented with respect to the lipid bilayer [74]. OPM database provides a useful guide about positioning proteins in membrane. Currently, there are about two thousand unique structures of membrane proteins available in OPM database. Structural orientations of proteins in OPM database were evaluated based on atomic solvation parameters implemented in an empirical energy function. For a quantitative evaluation of the PB method, a total of 1,060 structures of membrane proteins taken from OPM database were examined. The free energy profiles as a function of insertion depth of protein structure were obtained by varying positions of proteins along the membrane normal and permitting to spot the position with the lowest energy. The results are compared with the optimized position of membrane proteins in the OPM database. The present approach using the solvent

continuum model is expected to be of great assistance for building protein-lipid system suitable for experimental and computational studies of membrane proteins.

5.2 Background

The strategy is to compute the solvation energy of proteins inserted into the membrane at different depth and then locate the position for the minimum solvation energy. The implicit solvation model is a simple but present an efficient approach for the study. The Poisson-Boltzmann (PB) method is widely used for computing electrostatic contributions to free energies of solvation of biomolecular systems. The relation between the electric potential and the charge distribution in the presence of electrolyte solution is given by the PB equation (PBE)

$$\nabla \cdot \varepsilon(\vec{r})\nabla\Phi(\vec{r}) = -\rho(\vec{r}), \tag{5.1}$$

Where ε is the dielectric constant, Φ is the electric potential with a spatial charge distribution (ρ) or the charge density. All three variables are position-dependent functions represented by the position vector r. By considering the situation where the protein solute dissolved in an electrolyte media, the charge density in the solution at temperature T obeys a Boltzmann distribution. The Poisson-Boltzmann equation (PBE) may be re-written as

$$-\nabla \cdot [\varepsilon(\vec{r})\nabla\phi(\vec{r})] + \bar{\kappa}^2(\vec{r})sinh[\phi(\vec{r})] = -\frac{e}{k_B T}4\pi\rho(\vec{r}), \tag{5.2}$$

Where $\phi = e\Phi/k_B T$ is the reduced electrostatic potential. κ^2 is the Debye-Hückel screening parameter, which accounts for ionic shielding. For a given protein configuration and dielectric constants of solute environment, Φ can be obtained and the total electrostatic energy is determined the sum over all charges in the system. Solving the PBE gives rise to the electrostatic free energy according to

$$\Delta G_{elec} = \sum \Phi(\vec{r})\rho(\vec{r}), \tag{5.3}$$

The ΔG_{elec} in Eq. (5.3) indicates an amount of the electrostatic reversible work required to transfer the solute in a given configuration from vacuum to solution. To examine the membrane solvation energy, the relative value of ΔG_{elec} is considered. By assuming a fix configuration, the delta of ΔG_{elec} is obtained by subtracting the electrostatic solvation energy of the protein computed with a low-dielectric membrane-like environments $\Delta G_{elec,membrane}$ from that computed with a high dielectric water media ($\Delta G_{elec,water}$). The electrostatic free energy of membrane solvation ($\Delta\Delta G_{elec}$) can be obtained by solving PBE for the protein in different solvent environments (Figure 5.1)

$$\Delta\Delta G_{elec} = \Delta G_{elec,membrane} - \Delta G_{elec,water} \tag{5.4}$$
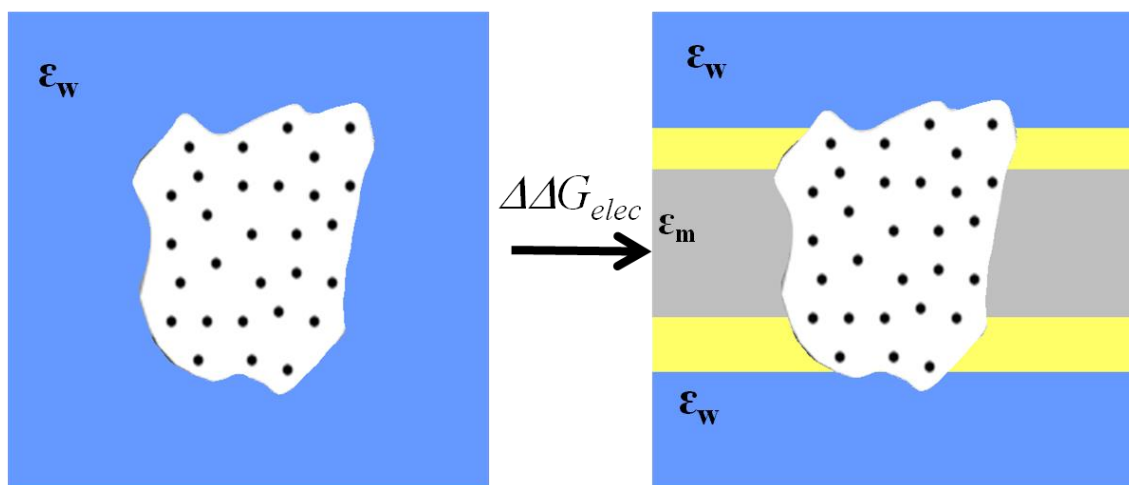
Figure 5.1 Calculation pathway of the electrostatic free energy.

5.3 Methods

5.3.1 Selecting proteins for validation

Before conducting an extensive computation with a large set of proteins, structures of six transmembrane proteins were used for validating the method, and thus taken directly from Protein Data Bank to avoiding bias results. The tested

proteins include isolated voltage sensor domain (VSD) of KvAP (1ORQ), KcsA (1K4C), Kv1.2-2.1 chimera (2R9R), Large-Conductance Mechanosensitive channel (2OAR), the voltage sensor domain of NaVAb (3RVY) and CorA Mg transporter (2IUB). These chosen transmembrane proteins are a class of multimeric protein channels. Therefore, transmembrane domains of these proteins are well identified and importantly spatial arrangement in the xy-plane (presumably the lipid bilayer) is simply estimated based on the orientation of the pore along the z-axis.

5.3.2 Pre-orienting and generating positional configurations of tested proteins

In the first step, protein structures were moved so that the center of mass lies at the origin (0,0,0). Then, the structures was rotated in a way that the central pore axis is perpendicular to the membrane plane. In other words, the pore axis of the protein channels is aligned with the z-axis. After pre-orienting the structure, the only one orientational parameter remaining to be determined is the position of the protein in the z-axis.

Transformation of atomic coordinates were done using the program VMD and tcl-command scripts. For each protein model, a set of structure coordinates was generated in accordance with a translation of the protein center of mass along the z-axis. The z-positions of the protein structure were varied in a range of 45-50 Å with an increment of 1 Å. This gave rise to a total of 45-50 positional configurations per protein to be systematically examined by calculatiing of the transfer free energy of solvation. It should be noted that by defining a membrane-spanning region in the calculated system, each generated configuration captures levels of the depth for proteins penetrating into the membrane-like environment.

5.3.3 Calculating electrostatic free energy of solvation

The program PDB2PQR was used to add hydrogen atoms and assign atomic charges and radii to each generated configuration. Partial atomic charges and radii of the protein were taken from the PARSE parameter sets. The sequential focusing multigrid algorithm in solving PBE consists of three resolution maps:

$300\times300\times300$ Å^3 for coarse, $200\times200\times200$ Å^3 for medium, and $100\times100\times100$ Å^3 for fine resolutions. Grid points of $161\times161\times161$ were employed to all maps. The implicit membrane slab was introduced such that its plane is in the Cartesian xy-plane and the bilayer normal is aligned along the z-axis. A thickness of membrane bilayer (L_{mem}) was evaluated between 30-40 Å. The dielectric constants for the membrane (ε_m) and water (ε_m) was 2 and 80, respectively (Figure 5.3).The low-dielectric slab accounting for hydrophobic membrane region and its thickness were defined by the z-value.The dielectric constant of protein was varied between 2, 4 and 10. Ionic strength was 0.1 M with coulomb charge +1 and -1, and radius 2.0 Å. Water probe radius was 1.4 Å. The calculations were performed by using the program Adaptive Poisson-Boltzmann Solver (APBS) 1.2.1 [75] with help of a java-based graphical user interface APBSmem for setting up input parameters [59]. For each configuration, the electrostatic free energy of solvation was computed twice, one for implicit aqueous model and one for water-lipid model, giving rise to $\Delta G_{elec,water}$ and $\Delta G_{elec,membrane}$, respectively. The transfer free enrgy ($\Delta\Delta G_{elec}$) that is the electrostatic free energy difference of the proteins embedded in the two solvent environments was obtained according to Eq.(5.4).

5.3.4 Examining the database

Further validation of the method was achieved by examining a large structure dataset of proteins in a membrane protein structure database. In this study, a total of 1,060 membrane protein structures taken from Orientations of Proteins in Membranes (OPM) database was chosen for calculating the test the method. The tested membrane proteins in this dataset were grouped according to protein classification in OPM database. There are five classes; α-helical polytopic, α-helical bitopic, β-barrel, α-helical peptide and monotopic/peripheral (Figure 5.2).The first three classes are a type of transmembrane proteins whereas the last two classes are a type of peripheral/monotopic proteins and petides. This classification is based on the secondary structure characters of transmembrane segments or membrane-associated domain.

The coordinate system applied to this study has the same reference frame used in OPM database and structures of the tested proteins were pre-oriented with respect to the bilayer. Therefore, structural data taken from the database were used directly as the starting configuration without further rotation and translation along the x- and y-axes. The only translation along the z-axis is required in order to search for the minimum energy position using the PB method. Unless otherwise specified, the whole protein structures were translated along the z-axis in a range of ±5 Å from their initial position with an increment of 1 Å. This gave rise to a total of 11 positional configurations per protein or over 12,000 configurations to be computed. Calculations of the transfer free energy were achieved using the APBS and APBSmem programs with the same protocol described previously.
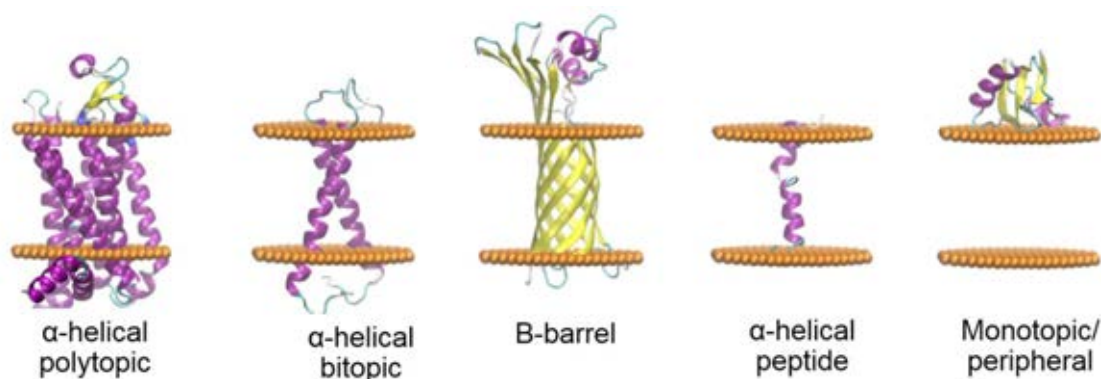
Figure 5.2 There are five classes of proteins in OPM database

5.4 Results and discussion

5.4.1 Positioning six protein channels in membrane

Figure 5.3 shows the computed energy profiles of six protein channels as a function of penetration depth. The PB electrostatic free energy of solvation is presented as relative $\Delta\Delta G_{elec}$ with respect to the lowest value within the tested protein. All the energy profiles of tested proteins allow easily spotting the position at the lowest energy. Visualization of protein structures at the lowest-energy configurations revealed a nice fitness of transmembrane domains of all tested protein within membrane boundary. The energy profiles of membrane insertion also suggested that if

the major part of transmembrane domains is located within membrane boundary, they tend to give the relatively low value of Δ_{Gelec}. In addition, a statistical analysis of positional tolerance showed that the z-distance shift with an average of ± 1 Å from the energy-minimum position produced the energy difference between the shifted and lowest-energy positions less than 5% of $\Delta\Delta G_{elec,lowest}$. Therefore, the energy tolerance due to the z-position shift may be considered as an allowable deviation for the positional refinement using the present approach.
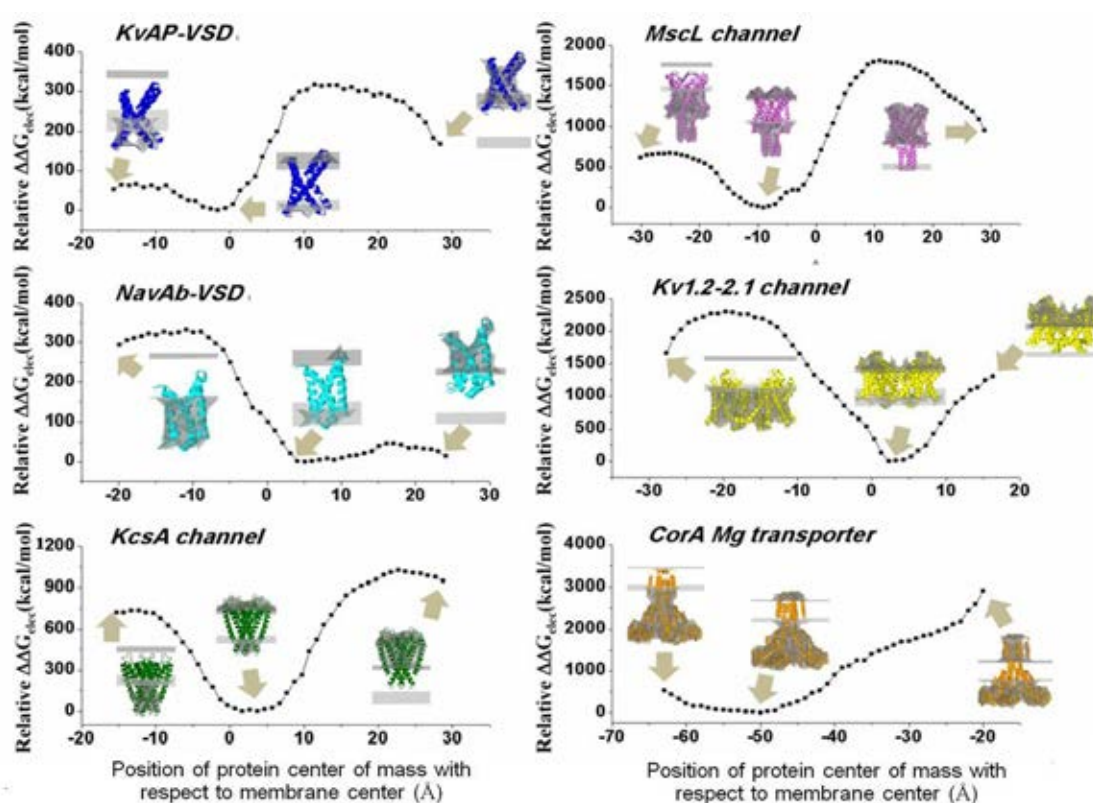
Figure 5.3 Six transmembrane proteins and their corresponding solvation energy as a function of position measured by distance between protein center and membrane normal center.

5.4.2 Examining positions of proteins from OPM database

A total of 1060 structures taken from OPM database were examined. For each examined protein, 11 configurations   To calculate the $\Delta\Delta G_{elec}$ profiles, a similar protocol was used. Regarding the availability of structural data, the numbers of

proteins to be exmined in each class were 285 for α-helical polytopic proteins, 64 for α-helical bitopic proteins, 33 for β-barrel proteins, 214 for α-helical peptide and 464 for monotopic/peripheral proteins. Percent distribution of tested proteins of each class was graphically shown in Figure 5.4.
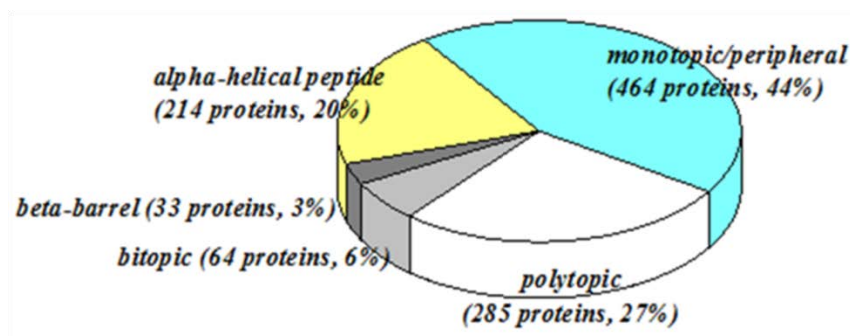
Figure 5.4. Percent distribution of tested proteins

5.4.2.1 Evaluation of $\Delta\Delta G_{elec}$ profiles

The transfer free energy ($\Delta\Delta G_{elec}$) calculations conduced over a thousand tested proteins suggested that the PB method provides useful guide for positioning membrane proteins in the lipid bilayer. The majority of $\Delta\Delta G_{elec}$ profiles obtained by the method allow one to pinpoint the minimum energy position in the lipid bilayer for the three classes of transmembrane proteins while the $\Delta\Delta G_{elec}$ curves belonging to the peripheral/monotopic proteins and peptides have no minimum point. Figure 5.5 highlighted the patterns of $\Delta\Delta G_{elec}$ profiles most commonly found in each membrane protein class. For α-helical polytopic protein, a parabolic-like curve of $\Delta\Delta G_{elec}$ profiles near the minimum energy was frequently observed. The α-helical bitopic and β-barrel transmembane proteins also exhibited a similar U-like shape of $\Delta\Delta G_{elec}$ profiles, but less frequent for the α-helical bitopic class. The results can be explained in terms of hydrophobic effect of non-polar solvent. In polytopic and β-barrel proteins, it is most often formed a well-packed bundle of hydrophobic transmembrane segments. The $\Delta\Delta G_{elec}$ profiles, therefore, showed a parabolic-like arc near the minimum. However, it was found that the U-like shape of $\Delta\Delta G_{elec}$ profiles near the minimum was not observed for many tested proteins in the bitopic class.A closer look

at structure and spatial arrangement of bitopic α-helical transmembrane proteins used in the study revealed a variety of structural forms. Some are monomeric or dimeric membrane anchors of a single transmembrane helix but many are extracellular and/or cytoplasmic parts without transmembrane segment. Therefore, the results of bitopic transmembrane proteins must be carefully interpreted. It was found that in this dataset there are 12 bitopic membrane proteins that consist of homo-or heterodimeric forms of a single transmembrane helix.

The influence of the polar face of transmembrane helices exposed to hydrophobic part of the lipid results in an unfavorable transfer free energy. For the peripheral/monotopic proteins and peptides, the $\Delta\Delta G_{elec}$ profiles do not behaves as a parabolic curve, indicating no minimum-energy position. As opposed to transmembrane protein type, these proteins partially contact to the membrane. For this reason, an increase of the transfer free energy can be described in terms of hydrophobic mismatch between the membrane and the inserted proteins/peptides.
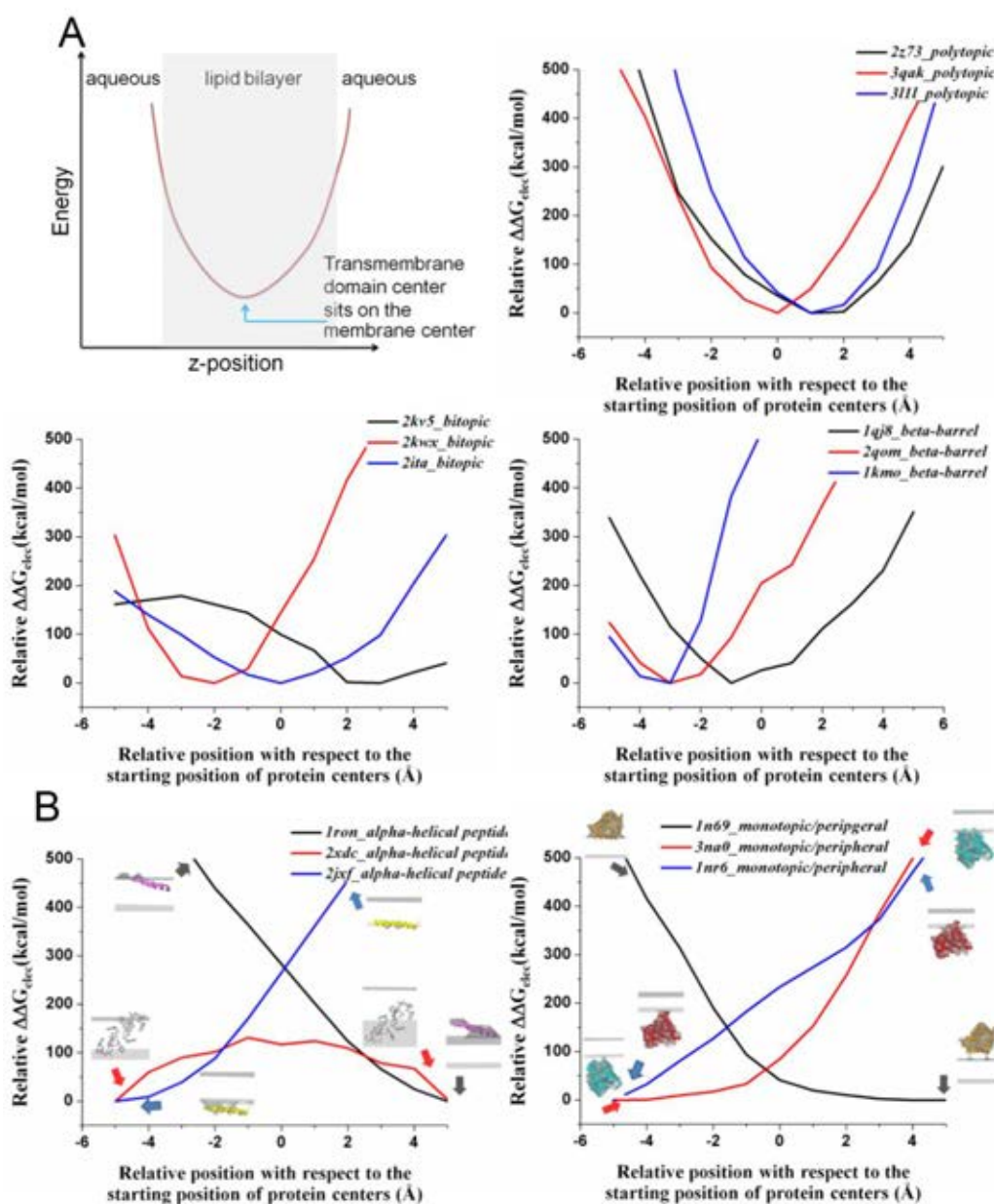
Figure 5.5 A) The majority of $\Delta\Delta G_{elec}$ profiles obtained the minimum energy position in the lipid bilayer consistent with three classes of proteins whereas B) two classes of proteins not found the minimum point present with the position of individual protein

All the $\Delta\Delta G_{elec}$ profiles of 1060 proteins in five classes were compiled to give a more comprehensive statistic data (Figure 5.6). Here, percentage of success test is determined. In case of transmembane proteins (polytopic, bitopic and β-barrel), a successful test is accounted by the use of the PB method being capable of finding the

minimum-energy position from the $\Delta\Delta G_{elec}$ profile. 87% of 285 α-helical polytopic proteins, 33% of 64 α-helical bitopic proteins and 79% of β-barrel proteins were considered as a successful test. The $\Delta\Delta G_{elec}$ profiles of peripheral/monotopic proteins and petides cannot be described by the parabolic-like behavior because the proteins do not have transmembane segment, implying no proper position in the lipid bilayer. However, the PB method can be considerably useful to distinguish between transmembrane proteins and membrane proteins without transmembrane domain. As can be seen in Figure 5.6., more than 90% of the tested proteins (94% of α-helical peptide and 99% of peripheral) do not have a parabolic-like shape.
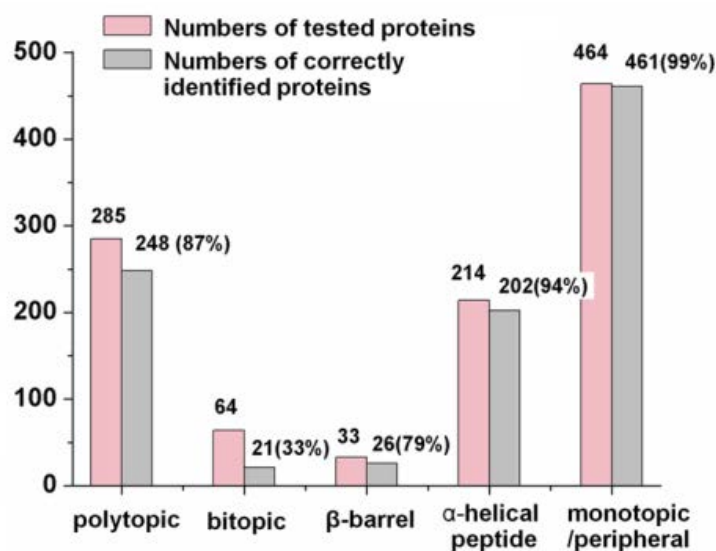
Figure 5.6 The $\Delta\Delta G_{elec}$ profiles of 1060 proteins in five classes

5.4.2.2 Minimum-energy position
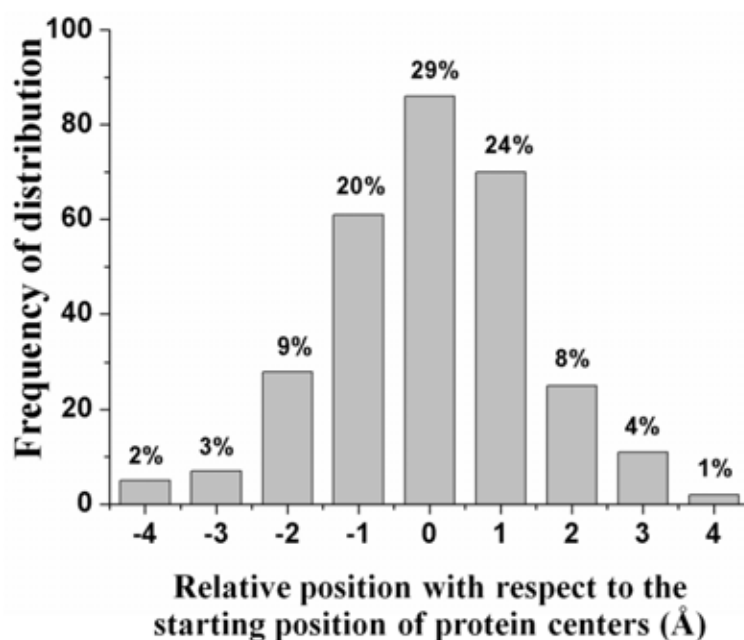
Figure.5.7 The frequency distribution of the minimum energy positions relative with the starting position of protein center

It should be noted that structure of the tested protein taken from OPM database centers the position at zero. A histogram shown in Figure 5.7 illustrates a frequency distribution of the minimum-energy positions relative to the starting position of protein centers. The frequency at the zero position indicates that the optimal position obtained by the present approach is consistent to that obtained in OPM database. By taking into account the allowable deviation of ± 1 Å, the sum of frequency distribution is equal to 73%. This result suggested the reliability of the present approach.

5.5 Conclusion

From the results, this study has shown that the solvent continuum PB method for calculating membrane solvation is useful for obtaining a proper position of membrane protein in the lipid bilayer. This approach is simple and fast because of an implicit treatment of solvent model. This approach can be of great assistance in setting up an initial configuration for molecular dynamics simulation of membrane protein in an explicit solvent.

CHAPTER VI
CONCLUSION

This thesis study is focused on structural and dynamical properties of voltage sensor domain (VSD) of voltage-gated KvAP potassium channel in the activated ("Up" or "Open") and the resting ("Down" or "Closed") conformations by means of computational approaches. The work aimed to evaluate the Down-state conformation constructed using the x-ray structure of the Up state of KvAP-VSD as the starting conformation and available experimental EPR data as constraints in molecular dynamics calculations. The Up and the best experimentally-fitted Down models of KvAP-VSD were evaluated by all-atom molecular dynamic (MD) simulations with the explicit hydrated phospholipid bilayer and the gating charge calculations in the presence and absence of external electric fields representing the membrane potential. The results of MD simulations revealed secondary and global structural stability, salt bridge interactions of the S4 arginines, water-filled creviced in voltage sensor core and the positional relocation of the gating charge arginines between the two conformations. Structure comparison, especially the relocation of the arginines, suggested the S4 undergoes a mechanism of "slide and rotate" of the helix. The gating charge responsible for such VSD motion was calculated to be $2.82\pm0.09e$ per monomer. This is in good agreement with the experimental estimates of $12-14e$ measured for the Shaker K^+ tetrameric channel.

During the thesis work, the use of Poisson-Boltzmann solvent continuum method for positioning proteins in membrane was examined. The aim is to calculate the different free energy of solvation for the tested proteins immerged in two solvent media (water and water-lipid) presented by high (for water) and low (for membrane) continuum dielectric slabs. The study was tested using 1060 membrane protein structures from Orientations of Proteins in Membranes (OPM) database. The free energy profiles as a function of insertion depth of protein structure were computed by varying positions of proteins along the membrane normal and permitting to spot the position with the lowest energy. By comparing with the optimized position of membrane proteins in the OPM database, the results showed a considerable success in

an accurate prediction of the position with more than 73% of the tested proteins. It is anticipate that the present approach be of great assistance in setting up an initial configuration for molecular dynamics simulation of membrane protein in an explicit solvent.

REFERENCES

[1]   Yeagle, L. P. Lipid regulation of cell membrane structure and function.
        <u>FASEB</u>. 3 (May 1989): 1833-1842.

[2]   Peck, T.; Hill, S., and Williams, M. Drug passage across the cell membrane.
        <u>Pharmacology for Anaesthesia and Intensive Care</u>. 3 (January 2008):
        1-10.

[3]   Alberts, B.; Johnson, A.; Lewis, J.; Roberts, K., and Walter, P. <u>Molecular
        biology of the cell</u>. 5 (2008): 1-94.

[4]   Singer, J. S., and Nicolson, L. G. The fluid Mosaic model of the structure of
        cell membranes. <u>Science.</u> 175 (February 1972): 720-731.

[5]   Shannon, T. Membrane function and structure and an introduction to
        membrane transport of solutes. <u>Membrane transport self study</u>. 3-18.

[6]   Structural biochemistry/membrane proteins/passive transport. [online]. 2011.
        Available from: http://www.en.wikibooks.org/wiki/Structural_Bio-
        Chemistry/Membrane_Proteins/Passive_Transport [2011, January]

[7]   Miller, M. D. The osmotic pump theory of selective transport. <u>Biochim.
        Biophys. Acta</u>. 37 (April 1960): 448-462.

[8]   Kjelstrup, S.; Rubi, M. J., and Bedeaux, D. Active transport: a kinetic
        description based on thermodynamic grounds. <u>J. Theor. Biol.</u> 234
        (November 2004): 7-12.

[9]   Smith, P. N., and Crampin, J. E. Development of models of active ion
        transport for whole-cell modeling: cardiac sodium-potassium pump as
        a case study. <u>Progress in Biophysics & Molecular Biology</u>. 85
        (January 2004): 387-405.

[10]   Inesi, G. Teaching active transport at the turn of the twenty-first century:
        recent discoveries and conceptual changes. <u>Biophysics. J</u>. 66 (March
        1994): 554-556.

[11]   Terlau, H., and Stuhmer, W. Structure and function of voltage-gated ion
        channels. <u>Naturwissenschaften</u>. 85 (1998): 437-444.

[12]   Choe, S. Potassium channel structures. <u>Nat. Rev.</u> 3 (February 2002):
        115-121.

[13]   Horn, R. Coupled movements in voltage-gated ion channels. <u>J. Gen. Physiol</u>.
       120 (October 2002): 449-453.

[14]   Sansom, S. P. M.; Shrivastava, H. I.; Bright, N. J.; Tate, J.; Capener, E. C.,
       and Biggin, C. P. Potasium channels: structure, models, simulations.
       Biochim. <u>Biophys. Acta</u>. 1565 (July 2002): 294-307.

[15]   Jegla, T.; Zmasek, M. C.; Batalov, S., and Nayak, K. S. Evoluation of the
       human ion channel set. <u>Comb. Chem. High Throughput Screen</u>. 12
       (2009): 2-23.

[16]   Salkoff, L.; Wei, D. A.; Baban, B.; Butler, A.; Fawcett, G.; Ferreira, G., and
       Santi, M. C. Potassium channels in C. elegans. WormBook.org.
       (December 2005): 1-15.

[17]   North, A. R. Famillies of ion channels with two hydrophobic segments.
       <u>Current Opinion in Cell Biology</u>. 8 (1996): 474-483.

[18]   Lehmann-Honn, F., and Jurkat-Rott, K. Voltage-gated ion channels and
       hereditary disease. <u>Physiological reviews</u>. 79 (October 1999): 1317-
       1355.

[19]   Avinash, S. Ion channels-a brief overview. [online]. 2011. Available from:
       http://www.http://exploreable.wordpress.com/2011/10/19/ion-
       channels-a-brief-overview/ [2011, October]

[20]   Alberts, B.; Johnson, A.: Lewis, J.; Raff, M.; Roberts, K., and Walter, P.
       <u>Molecular Biology of the cell</u>. 4th ed. 2002.

[21]   Berridge, J. M. Ion channels. Cell Signalling Biology. [online]. 2012.
       Available from:http://www.cellsignallingbiology.org/csb/
       003/csb003.pdf [2012]

[22]   Sengupta, B.; Stemmler, M.; Laughlin, B. S., and Niven, E. J. Action potential
       energy efficiency varies among neuron types in vertebrates and
       invertebrates. <u>PLoS Comput Biol</u>. 6 (July 2010): 1-16.

[23]   Bean, P. B. The action potential inmammalian central neurons.
       <u>Nat. Rev.</u> 8 (June 2007): 451-465.

[24]   Kappen, B. Introduction to biophysics. [online]. 2008. Available from:

       http://www.snn.rn.nl/bertk/biofysica/handouts.pdf [2008, February]

[25]   Aizenmen, L. Principles of neurobiology. [online]. 2012. Available from:
       http://wiki.brown.edu/confluence/display/Spring07MN0102S01/Ion
       +Channel+Function [2010, February]

[26]   Wright, H. S. Generation of resting membrane potential. Advan. Physiol.
       Educ. 28 (September 2004): 139-142.

[27]   Barnett, W. M., and Larkman, M. P. The action potential. Pract. Neurol. 7
       (2007): 192-197.

[28]   Matthews G. Neurobiology: Molecules, Cells and Systems. Science. (1998)

[29]   Yu, H. F.; Yarov-Yarovoy, V.; Gutman, A. G., and Catterall, A. W. Overview
       of molecular relationships in the voltage-gated ion channel
       superfamily. Pharmacol. Rev. 57 (2005): 387-395.

[30]   Marban, E. Cardiac channelopathies. Nature. 415 (January 2002): 213-218.

[31]   Nau. C. Voltage-gated ion channels. Handbook of Experimental
       Pharmacology. 182 (2008): 85-92.

[32]   Anderson, A. V. P., and Greenberg, M. R. Phylogeny of ion channels: clues to
       structure and function. Comparative Biochemistry and Physiology. 129
       (February 2001): 17-28.

[33]   Tombola, F,;Pathak, M. M., and Isacoff, Y. E. How does voltage open an ion
       channel?. Annu. Rev. Cell Dev. Biol. 22 (May 2007): 23-52.

[34]   Swartz, J. K. Sensing voltage across lipid membranes. Nature. 456 (December
       2008): 891-897.

[35]   Catterall, A. W.; Cestele, S.; Yarov-Yarovoy, V.; Yu, H. F.; Konoki, K., and
       Scheuer, T. Voltage-gated ion channels and gating modifier toxins.
       Toxicon. 49 (September 2007): 124-141.

[36]   MacKinnon, R. Potassium channels. <u>FEBS Letters</u>. 555 (October 2003): 62-65.

[37]   Borjesson, I. S., and Elinder, F. Structure, function, and modification of the voltage sensor in voltage-gated ion channels. <u>Cell Biochem. Biophys</u>. 52 (November 2008): 149-174.

[38]   Schow, V. E.; Freites, A. J.; Gogna, K.; White, H. S., and Tobias, J. D. Down-state model of the voltage-sensing domain of a potassium channel. <u>Biophys. J</u>. 98 (June 2010): 2857-2866.

[39]   Shieh, C.; Coghlan, M.; Sullivan, P. J., and Gopalakrishnan, M. Potassium channels: molecular defects, deseases, and therapeutic opportunities. <u>Pharmacol Rev</u>. 52 (2000): 557-593.

[40]   Jiang, Y.; Lee, A.; Chen, J.; Ruta, V.; Cadene, M.; Chait, T. B., and MacKinnon, R. X-ray structure of a voltage-dependent K$^+$ channel. <u>Nuture</u>. 423 (May 2003): 33-41.

[41]   Andersson, M.; Freites, A. J.; Tobias, J. D., and White, H. S. Structural dynamics of the S4 voltage-sensor helix in lipid bilayers lacking phosphate groups. <u>J. Phys. Chem. </u>115 (June 2011): 8732-8738.

[42]   Cohen, E. B.; Grabe, M., and Jan, Y. L. Answers and questions from the KvAP structures. <u>Neuron. </u>39 (July 2003): 395-400.

[43]   Bezanilla, F. Voltage-gated ion channels. <u>IEEE</u>. 4 (March 2005): 34-48.

[44]   Darman, R.; Ivy, A., and Ketty, V. Constraints on voltage sensor movement in the shaker K+ channel. <u>Nature</u>. 371 (2006): 156-161.

[45]   Murata, Y.; Iwasaki, H.; Sasaki, M.; Inaba, K., and Okamura, Y.
          Phosphoinositide phosphatase activity coupled to an intrinsic voltage
          sensor. Nature. 435 (May 2005): 1239-1243.

[46]   Sasaki, M.; Takagi, M., and Okamura, Y. A voltage sensor-domain protein is a
          voltage-gated proton channel. Science. 312 (April 2006): 589-592.

[47]   Li, J. Basic molecular dynamics. Handbook of Materials Modeling. (2005):
          565-588.

[48]   Gonzalez, M. A. Force fields and molecular dynamics simulations. EDP
          Science. 12 (2011): 169-200.

[49]   Meller, J. Molecular dynamics. Nature. (2001):1-8.

[50]   Maple, R. J.; Dinur, U., and Hagler, T. A. Derivation of force fields for
          molecular mechanics and dynamics from ab initio energy surfaces.
          PNAS. 85 (August 1988): 5350-5354.

[51]   Tieleman, P. D.; Marrink, J. S., and Berendsen, H. J. C. A computer
          perspective of membranes: molecular dynamics studies of lipid bilayer
          systems. Biochim. Biophys. Acta. 1331 (July 1997): 235-270.

[52]   Raychaudhuri, S. Introduction to monte carlo simulation. IEEE. (2008): 91-
          100.

[53]   Gunsteren, V. F. W., and Berendsen, C. J. H. Computer simulation of
          molecular dynamics: methodlgy, applications, and perspectives in
          chemistry. Angew. Chem. Int. Ed. Engl. 29 (1990): 992-1023.

[54]   Ryckaert, J. P.; Ciccotti, G., and Berendsen, C. J. H. Numerical integration of
        the Cartesian equations of motion of a system with constraints:
        molecular dynamics of n-alkanes. J. Comput. Phys. 23 (July 1977):
        327-341.

[55]   Omelyan, P. I. Algorithm for numerical integration of the rigid-nody equations
        of motion. PACS. (January 1999): 1-4.

[56]   Mackerell, D. A. Empirical force fields for biological macromoleculrs:
        overview and issues. J. Comput. Chem. 25 (May 2004): 1584-1604.

[57]   Fogolari, F.; Brigo, A., and Molinari. H. The Poisson-Boltzmann equation for
        biomolecular electrostatics: a tool for structural biology. J. Mol.
        Recogn. 15 (July 2002): 377-392.

[58]   Pang, X., and Zhou, H. Poisson-Boltzmann calculations: van der walls or
        molecular surface?. Commun. Comput. Phys. 13 (January 2013): 1-12.

[59]   Callenberg, M. K.; Choudhary, P. Om.; Forest, de. L. G.;Gohara, W. D.;
        Baker, A. N., and Grabe, M. APBSmem: a graphical interface for
        electrostatic calculations at the membrane. PLoS ONE. 5 (September
        2010): 1-11.

[60]   Honig, B., and Nicholls, A. Classical electrostatics in biology and chemistry.
        Science. 268 (May 1995): 1144-1149.

[61]   Schaefer, M., and Karplus, M. A comprehensive analytical treatment of
        continuum electrostatics. J. Phys. Chem. 100 (October 1996): 1578-
        1599.

[62]   Wang, J.; Tan, C.; Tan, Y.; Lu, Q., and Luo, R. Poisson-Boltzmann solvents in
        molecular dynamics simulations. Commun. Comput. Phys. 3 (May
        2008): 1010-1031.

[63]   Goncalves, B. F. P, and Stassen, H. Calculation of the free energy of salvation
           from molecular dynamics simulations. <u>Pure Appl. Chem.</u> 76
           (September 2004): 231-240.

[64]   Dong, F.; Olsen, B., and Baker, A. N. Computational methods for
           biomolecular electrostatics. <u>Meth Cell Biol</u>. 84 (2008):
           843-870.

[65]   Taheri-Araghi, S., and Ha, B. Electrostatic bending of lipid membranes: how
           are lipid and electrostatic properties interrelated? <u>Langmuir.</u> 26 (July
           2010): 14737-14746.

[66]   Hsu, J., and Liu, B. Exact solution to the linearized Poisson-Boltzmann
           equation for spheroidal surfaces. <u>Adv. Colloid interface Sci.</u>
           175 (March 1996): 785-788.

[67]   Sharp, A. K., and Honig, B. Calculating total electrostatic energies with the
           nonlinear Poisson-Boltzmann equation. <u>J. Phys. Chem.</u> 94 (May
           1990): 7684-7692.

[68]   Li, Q.; Jogini, V.; Wanderling, S.; Cortes, D., and Perozo, E. Expression,
           purification, and reconstitution of the voltage-sensing domain from Ci-
           VSP. <u>Biochemistry</u>. 41 (October 2012): 8132-8142.

[69]   Freites, A. J.; Tobias, J. D., and White, H. S. A voltage-sensor water pore.
           <u>Biophys. J.</u> (September 2006): 90-92.

[70]   Chakrapani, S.; Cuello, G. L.; Cortes, M. D., and Perozo, E. Structural
           dynamics of an isolated voltage-sensor domain in a lipid bilayer.
           <u>Structure</u>. 16 (March 2008): 398-409.

[71]   Sompornpisut, P.; Roux, B., and Perozo, E. Structural refinement of
        membrane proteins byrestrained molecular dynamics and solvent
        accessibility data. <u>Biophys. J</u>. 95 (December 2008), 5349–5361.

[72]   Zheng, H.; Liu, W.; Anderson, Y. L., and Jiang, Q. Lipid-dependent gating of
        a voltage-gated potassium channel. <u>Nat. Commun</u>. 10 (March 2011):
        1-9.

[73]   Gumbart, J.; Khalili-Araghi, F.; Sotomayor, M., and Roux, B. Constant
        electric field simulations of the membrane potential illustrated with
        simple ststems. <u>Biochim. Biophys. Acta</u>. 1818 (February 2012):294-
        302.

[74]   Lomize, L. A.; Pogozheva, D. P.; Lomize, A.M., and Mosberg, I. H.
        Positining of proteins in membranes: a computational approach.
        <u>Protein Science</u>. 15 (February 2006): 1318-1333.

[75]   Baker, N; MaCammon, J. A.; Holst, M. Adaptive Poisson-Boltzmann
        solver.[Online]. 2010. Available from :
        http://www.poissonboltzmann.org[October, 2010]

APPENDIX

Programming A.1 Analysis script backbone RMSD and RMSF

```
set initmol [mol load psf ../../02membrane/protein_popcwi.psf pdb
../../02membrane/protein_popcwi.pdb]

set outfile [open "rmsd.dat" w]
set initmol [mol load psf ../../02membrane/protein_popcwi.psf pdb
../../02membrane/protein_popcwi.pdb]

set outfile [open "rmsd.dat" w]
set frame0 [atomselect $initmol "alpha" frame 0]

set trajmol [mol load psf ../../02membrane/protein_popcwi.psf dcd
../dcd/protein_popcwi-01.dcd]
foreach no { 02 03 04 05 06 07 08 09 10 11 12 } {
mol addfile ../dcd/protein_popcwi-$no.dcd type dcd first 0 last -1 waitfor all
}

set nf [molinfo $trajmol get numframes]
set selref [atomselect $trajmol "alpha"]
set sel [atomselect $trajmol "alpha"]
set prot [atomselect $trajmol "protein" ]
# rmsd calculation loop
for {set i 1 } {$i < $nf } { incr i } {
   $selref frame $i
   $sel frame $i
   $prot frame $i
   $sel move [measure fit $selref $frame0]
   $prot move [measure fit $selref $frame0]
   puts $outfile   "$i : [measure rmsd $sel $frame0]"
}

set fp [open "rmsf.dat" w]
#set sel [atomselect $trajmol "alpha"]
for {set i 0} {$i < [$sel num]} {incr i} {
 set rmsf [measure rmsf $sel first 1 last 3000 step 10]
 puts $fp "[expr {$i+20}] [lindex $rmsf $i]"
}
close $fp
```

Programming A.2 NAMD input file

```
structure           ../02membrane/protein_popcwi.psf
coordinates         ../02membrane/protein_popcwi.pdb
outputName          protein_popcwi-01
set temperature     298
# Continuing a job from the restart files
if {0} {
setinputnameprotein_popcwi
binCoordinates      $inputname.restart.coor
binVelocities           $inputname.restart.vel  ;# remove the "temperature" entry if you use
this!
extendedSystem      $inputname.restart.xsc
}firsttimestep       0


## SIMULATION PARAMETERS                          ##
# Input paraTypeCharmm      on
parameters          ../par_all27_prot_lipid.inp

# NOTE: Do not set the initial velocity temperature if you
# have also specified a .vel restart file!
temperature         $temperature

# Periodic Boundary Conditions
# NOTE: Do not set the periodic cell basis if you have also
# specified an .xsc restart file!
if {1} {
cellBasisVector1    79.  0.  0.
cellBasisVector2     0.  78.  0.
cellBasisVector3     0.   0.  81.
cellOrigin0.009354357607662678 0.33048391342163086 0.029091475531458855
wrapWater           on
wrapAll             on

# Force-Field Parameters
exclude             scaled1-4
1-4scaling          1.0
cutoff              12.
switching           on
switchdist          10.
pairlistdist        13.5

# Integrator Parameters
timestep            2.0  ;# 2fs/step
rigidBonds          all  ;# needed for 2fs steps
nonbondedFreq       1
fullElectFrequency  2
stepspercycle       20
```

```
#PME (for full-system periodic electrostatics)
if {1} {
PME             yes
PMEGridSizeX     100
PMEGridSizeY     100
PMEGridSizeZ     90
}
# Constant Temperature Control
langevin         on    ;# do langevin dynamics
langevinDamping   1    ;# damping coefficient (gamma) of 5/ps
langevinTemp      $temperature

# Constant Pressure Control (variable volume)
if {1} {
useGroupPressure      yes ;# needed for 2fs steps
useFlexibleCell       yes  ;# no for water box, yes for membrane
useConstantArea       no  ;# no for water box, yes for membrane

langevinPiston        on
langevinPistonTarget  1.01325 ;#  in bar -> 1 atm
langevinPistonPeriod  200.
langevinPistonDecay   50.
langevinPistonTemp    $temperature
}
restartfreq        1000     ;# 1000steps = every 2ps
dcdfreq            1000
xstFreq            1000
outputEnergies     50
outputPressure     50

## EXTRA PARAMETERS                          ##
# Put here any custom parameters that are specific to
# this job (e.g., SMD, TclForces, etc...)
#tclforces on
#set waterCheckFreq          100
#set lipidCheckFreq          100
#set allatompdb             ../02membrane/protein_popcwi.pdb
#tclForcesScriptkeep_water_out.tcl
#eFieldOn yes
#eField 0 0 -0.155

## EXECUTION SCRIPT                          ##
# Minimization
if {1} {
minimize          5000
reinitvels        $temperature
}
run 250000 ;# 0.5 ns
```

VITAE

Personal Data:

First Name: Miss Sunit   **Last Name:** Fuklang

Date of birth: December 11, 1987   **Height:** 155 cm.

Weight: 48 kg.   **Citizenship:** Thai

Religion: Buddhism   **Domicile/Habitation:** NakhonRatchasima

Gender: Female   **Primary Phone:** 083-3535915

E-mail address: nit_phychem1112@hotmail.com

Home Address: 343Top Top apartment Soi:18 Rama VI rood

District: Ratchathewi **State/Province:** Bangkok **Postal Code:** 10400

Country: Thailand

Education:

2010-Present: Master's Degree in Science , Major Chemistry (Physical chemistry) Chulalongkorn University, Thailand,GPA. 3.53/4

2006-2009: Bachelor's Degree in Science , Major Chemistry , KhonKaen University, Thailand, GPA. 3.34/4

2003-2005: High School from Soeng Sang school, Nakhonratchasima, Thailand

2002-2004: Junior High School from Nongsanuan school, Nakhonratchasima , Thailand

Research Interest:

2010-Present: Structural and dynamical properties of voltage sensor domain of activated and resting potassium channel in lipid bilayer by molecular dynamics simulation

2009:   Synthesis of titanium dioxide photocatalysis and used as a photosensitizer in the oxidation of the acid blue (AB29) dye by using sunlight.

The full paper (Proceeding) and publication:

2012: Use of Poisson-Boltzmann solvation energy to position a transmembrane protein in lipid bilayer for molecular dynamic simulation study